Spring 3-12-2017

A multi-proxy stalagmite reconstruction of the climate of southwestern North America from the Middle to Late Holocene

Christine Allen
University of New Mexico

Christine Allen
Candidate

Earth and Planetary Sciences
Department

This thesis is approved, and it is acceptable in quality and form for publication:

Approved by the Thesis Committee:

Yemane Asmerom, Chairperson

Victor Polyak

Louis Scuderi

A MULTI-PROXY STALAGMITE RECONSTRUCTION OF THE CLIMATE OF SOUTHWESTERN NORTH AMERICA FROM THE MIDDLE TO LATE HOLOCENE

BY

CHRISSY ALLEN

B.S. Geological Sciences, University of Florida, 2014

THESIS

Submitted in Partial Fulfillment of the
Requirements for the Degree of

Master of Science

Earth and Planetary Sciences

The University of New Mexico
Albuquerque, New Mexico

May 2017

ACKNOWLEDGEMENTS

I would first like to thank my advisor and thesis chair Dr. Yemane Asmerom for providing me the necessary support and motivation to complete this study and for his continuous guidance throughout my years of graduate study. I would also like to thank Dr. Victor Polyak for his support along the way and for the tremendous amount of time he spent teaching me in the lab as well as providing me with the opportunity to go caving. I would also like to thank Dr. Louis Scuderi for serving on my thesis committee and providing valuable feedback and support for this project.

Funding is from the National Science Foundation grant AGS-1503133.

A MULTI-PROXY STALAGMITE RECONSTRUCTION OF THE CLIMATE OF SOUTHWESTERN NORTH AMERICA FROM THE MIDDLE TO LATE HOLOCENE

by

Chrissy Allen
B.S., Geological Sciences, University of Florida, 2014
M.S., Earth and Planetary Sciences, University of New Mexico, 2017

ABSTRACT

The seasonal balance of moisture has a significant effect on natural ecosystems and culture in southwestern North America (SWNA), and it thus is necessary to understand the cause of this moisture variability in order to better predict the scope of potential future changes. Studies of modern SWNA climate indicate that most of the annual moisture at this site comes from monsoonal summer precipitation and a lesser amount of Pacific winter moisture. The climate of the Holocene is of particular interest for constraining natural variability of interglacial climates prior to any anthropogenic influence. An overall transition to a wetter Late Holocene climate in SWNA has been established by different climate proxies, and a definable shift in climate around 4.2 ka is observed in records from various locations around the world. However, the lack of highly resolved records in SWNA limits our ability to determine the mechanisms and timing of this climate shift in this region. In this study we present a high-resolution U-Th dated speleothem record from ~6500 to ~1000 yr BP of oxygen and carbon stable isotopes, Sr and Ba trace elements, grayscale, and $^{234}U/^{238}U$ isotope ratios from two caves in southeastern New Mexico. Our data suggests the climate of the Middle Holocene was warmer and dominated by monsoonal precipitation, and the Late Holocene was cooler

and experienced an increase in winter precipitation. Our record further suggests this shift occurred around 4.2 ka. High-frequency climate variability observed in SWNA during the Late Holocene has been attributed to an active ENSO/PDO system, yet this was limited by lack of direct comparison with the Middle Holocene. Spectral and wavelet analyses from this study show interdecadal and decadal variation observed in the Late Holocene that is not observed in the Middle Holocene, suggesting that strengthened ENSO/PDO activity is responsible for the increased moisture observed in SWNA during the Late Holocene by increasing winter precipitation.

TABLE OF CONTENTS

LIST OF FIGURES

LIST OF TABLES

CHAPTER 1 INTRODUCTION

How the earth will respond to increasing human-induced warming is one of the fundamental questions facing society globally, and how the response and impact of these rapid changes are likely to vary regionally is equally important. The impact of climate change on southwestern North America (SWNA) is expected to be significant if not severe given past records of climate-driven changes on the environment and culture (Hodell et al., 1995; deMenocal, 2001; Polyak and Asmerom, 2001; Haug et al., 2003; Asmerom et al., 2013). Understanding and characterizing past climates is an essential tool for predicting the effects of future climate variability. Of particular importance in this region is effective moisture, defined as precipitation minus evaporation. Previous speleothem, lake sediment, and tree ring studies (Antevs, 1955; Betancourt et al., 2001; Polyak and Asmerom, 2001; Menking et al., 2003; Rasmussen et al., 2006; Asmerom et al., 2007; Anderson et al., 2008) have documented significant climate variability in SWNA during the Holocene. A paleoclimate record of this time period from speleothem growth and oxygen isotope time-series shows a transition from a warmer and more arid early Middle Holocene to a cooler and wetter Late Holocene in SWNA (Polyak and Asmerom, 2001; Asmerom et al., 2007). The differences between the Middle and Late Holocene are subtle and require well-dated highly resolved records sensitive to these small differences.

SWNA has two rainy seasons (Metcalfe et al., 2015) with distinct summer versus winter moisture sources. The summer North American Monsoon (NAM) (Adams and Comrie, 1997) precipitation is sourced from the Gulf of Mexico and Gulf of California, whereas the winter moisture is derived from the Pacific Ocean. It is necessary to understand how the strength of these sources of moisture and their balance have varied with climatic changes over time in order to better determine how the effective moisture will respond to changes in future climate variability. The objective of this study is to construct a high-resolution climate record for the Middle to Late Holocene in SWNA and determine when a climatic transition occurred, and discuss the forcing mechanisms responsible for the transition observed in the speleothem record from SWNA. In addition, given that the Middle Holocene was notably warmer, this period should provide crucial information that can be used to predict climate sensitivities to future warming temperatures. This study uses three stalagmites from two different caves in the Guadalupe Mountains, New Mexico, U.S.A. that spans a period from 6500 to 1000 years before present (yr BP). The proxies represented by these stalagmites are oxygen and carbon stable isotopes, growth rates (banding and hiatuses), grayscale, elemental concentrations, and $^{234}U/^{238}U$ isotope ratios expressed as permil (‰) $\delta^{234}U$.

CHAPTER 2 BACKGROUND

2.1 Speleothem formation: from rainwater to soil to stalagmites

Speleothems have become essential for reconstructing Earth's climatic teleconnections because of their ability to produce continuous precise and absolute high-resolution chronologies and terrestrial paleoclimate records. Unlike ice cores they provide records from low latitudes and unlike marine cores they provide records of terrestrial climate. Preserved in them are an abundance of measurable paleoenvironmental proxies that are used in this study such as stable isotopes, trace elements, and growth bands that are used to interpret climatic and hydrologic processes of the past. Speleothem calcite deposition begins when rainwater infiltrates through the soil above the cave. As water flows through the epikarst and bedrock it dissolves CO_2 from plant/soil respiration and from the decay of organic matter and produces carbonic acid (Eq. 2.1).

$$H_2O + CO_{2(g)} \rightarrow H_2CO_{3(aq)} \tag{2.1}$$

After water moves through the soil it reaches limestone bedrock where some dissolution of the bedrock occurs (Eq. 2.2).

$$CaCO_{3(s)} + H_2CO_{3\,(aq)} \rightarrow Ca^{2+}{}_{(aq)} + 2HCO_3^-{}_{(aq)} \tag{2.2}$$

Finally, when carbonate-saturated water enters a cave where the air has a lower pCO$_2$ than the infiltrating water, CO_2 degasses from the water and the precipitation of speleothems occurs (Eq. 2.3).

$$Ca^{2+}{}_{(aq)} + 2HCO_3^-{}_{(aq)} \rightarrow CaCO_{3(s)} + CO_{2(g)} + H_2O \tag{2.3}$$

The entire process affects the geochemical composition of the resulting speleothem calcite.

2.2 Geologic Setting

There are over 300 known caves within the Guadalupe Mountains of southeastern New Mexico and western Texas. These caves lie within the northern margin of the Delaware Basin within the Permian Basin, which is composed of Permian-age reef deposits (Capitan limestone and associated backreef and forereef limestones and dolostones) and contains some of the country's largest oil fields (Hill, 2000). During the Miocene and through the Pliocene, hydrogen sulfide and carbon dioxide from the petroleum reservoirs mainly in the Delaware Basin migrated upward toward the water table of the Capitan aquifer along the Capitan reef rocks. These mixed with oxygen in the aquifer groundwater to form sulfuric and carbonic acid that dissolved the limestone and dolostone. This type of cave genesis where the aggressive components migrate from below is sulfuric acid hypogene speleogenesis. The majority of the dissolution thus occurred along the water table and has produced the large entrances and cavern chambers that are characteristic of these caves (Hill, 2000; Jagnow et al., 2000).

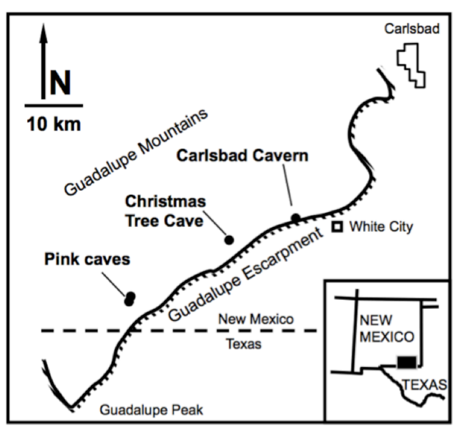

Figure 1 Schematic map showing cave locations in southeastern New Mexico. Stalagmites in this study were collected from Pink caves and Christmas Tree Cave.

2.3 Cave Setting

Speleothem samples were collected from two Guadalupe Mountain caves, Pink Dragon Cave and Christmas Tree Cave (Fig. 1). Both caves have large entrances that allow for exchange with the atmosphere, and both samples were collected from within 100 meters of those entrances.

In general, caves are relatively stable environments year round, where cave temperature and relative humidity are stable compared to the surface temperature and relative humidity (Rasmussen, 2006). For example, for Carlsbad Cavern the mean surface temperature is 63°F, while the cave temperature in much of the cave is 57°F (McLean, 1971). These caves with large entrances and passages that descend from the entrances create cold air sinks, explaining why the cave temperature is slightly lower than the mean annual surface temperature. The cave temperature in the deeper, more remote parts of Carlsbad Cavern is the same as the mean annual surface temperature of 63°F (McLean, 1971). Because cave environments mimic mean annual temperature and relative humidity it makes speleothems powerful recorders of terrestrial climate.

Christmas Tree Cave is located in Carlsbad Caverns National Park at an elevation of 1491 meters. The entrance to the cave is ~5 meters in diameter and consists of a 7-meter vertical drop to enter the cave. It opens up to a room ~8 meters tall and ~20 meters wide, and 15-20 meters deeper into the cave from the entrance drop is the site where the two samples for this study were collected. Both small columnar stalagmites grew 20 and 40 meters from the entrance in a well-ventilated area of the cave. Christmas Tree Cave is very well decorated with many types of speleothems; stalagmites, stalactites, huge columns, soda straws, helictites, and cave clouds.

Pink Dragon Cave is located on the Lincoln National Forest and its entrance is 1800 meters in elevation. The entrance is similar to that of Christmas Tree Cave, and the cave passage descends from the entrance to the passage where the sample was collected 50 meters into the cave and 20 meters below the entrance. Pink Dragon Cave is well decorated, and the cave setting is similar to Christmas Tree Cave.

The cave setting in Carlsbad Cavern where stalagmites BC2 and BC11 were collected and from which results were published by Polyak and Asmerom (2001) and Asmerom et al. (2013) is similar to that of Christmas Tree and Pink Dragon caves, except greatly up scaled.

These large entrance caves are considered evaporative relative to many other caves used in paleoclimate studies where relative humidity and air temperature do not fluctuate much (typically >95% and ±1°C) throughout the year. These conditions allow speleothem calcite to remain in equilibrium with the cave water percolating from the surface precipitation (McDermott, 2004; Lachniet, 2009). However, Rasmussen (2006) measured drip rate, temperature, and relative humidity in Carlsbad Cavern and demonstrated that these Guadalupe Mountain caves experience a larger annual temperature and relative humidity difference, reflecting seasonality observed on the surface. Carlsbad Cavern showed an annual relative humidity and temperature range of 90.5 – 69% and 8°-16.5°C respectively, demonstrating the role of ventilation in these large entrance caves. Annual banding in these small columnar stalagmites is evidence that stalagmite growth is continuous throughout each year recording both summer and winter seasons. Therefore, these seasonal, annual, decadal, and millennial changes are recorded in the stalagmites.

While this more evaporative cave environment would be considered less suitable by the majority of previous speleothem-based studies, a more evaporative cave environment is likely to reflect the conditions of the environment above the cave more directly. Thus, the extent that the climate of the surface environment changes seasonally, decadally, and millennially should be more directly recorded in the speleothem that grew during that time.

2.4 Sample Descriptions

Sample PD3 is a ~200 millimeter long stalagmite (Fig. 2) that shows slow but continuous growth from about 6000-2000 yr BP and grew through the Middle to Late Holocene transition. Sample X2 is a ~270 millimeter long calcite stalagmite (Fig. 3) that grew from about 6500-4000 yr BP, which represents the latter half of the Middle Holocene. Sample X3 is a ~280 millimeter long calcite stalagmite (Fig. 4) that grew from about 1900-950 yr BP and represents the core of the Late Holocene. Both stalagmites show comparable high growth rates, allowing them to be sampled for stable isotopes at near-annual resolutions. Their records can therefore be used to compare segments of the Middle and Late Holocene climate at a high resolution. Long-term paleoclimate information is represented by stalagmite PD3.

Figure 2 Stalagmite PD3 from Pink Panther Cave.

Figure 3 Stalagmite X2 from Christmas Tree Cave.

Figure 4 Stalagmite X3 from Christmas Tree Cave.

2.5 Modern Climate System in SWNA

SWNA is a semi-arid region where the amount of effective moisture is extremely sensitive to small changes in climate. Summer NAM precipitation is the dominant moisture source for this region as it accounts for more than half of the annual rainfall in the study area (Adams and Comrie, 1997). The NAM produces an increase in rainfall from late July to September in SWNA. At the start of monsoon season the Bermuda High, a subtropical high-pressure cell that typically sits south of the Azores in the eastern Atlantic Ocean, expands and migrates west toward SWNA. This in addition to intensified continental heating during the summer drives a monsoonal wind pattern (Adams and Comrie, 1997; Sheppard et al, 2002; Poore et al., 2005). By late July most of SWNA experiences increased rainfall due to clockwise circulation around the Bermuda High sweeping moisture into this region from the Gulfs of Mexico and California. The amount of effective moisture making it into the study area is also dependent on seasonal shifts in the relative position of the Intertropical Convergence Zone (ITCZ) that impacts the prevailing wind directions as well as the source of moisture in this region (Metcalfe et al., 2015).

During the El Niño months warming of the Northern Hemisphere causes the ITCZ to shift north, resulting in southeasterly winds moving across the gulfs (Poore et al., 2005) that enhance monsoon effects. In addition, during the winter months the ITCZ migrates down near the equator and the dominant winds are the Westerlies that bring moisture to this region from the Pacific. The winter moisture systems coming from the Pacific are driven by the polar jet stream, an active storm track that brings important precipitation for groundwater recharge to SWNA during winter months (Asmerom et al., 2010; Sheppard et al., 2002). Phases of El Niño Southern Oscillation (ENSO) and the Pacific Decadal Oscillation (PDO) enhance that precipitation (Rasmussen, 2006; McCabe et al., 2004).

2.6 Holocene Climate Variability

In general the climate of the Holocene is stable relative to the latter portion of the Pleistocene (Rasmussen et al., 2014). Temperature variation globally during the Holocene is only a few degrees Celsius (Marcott et al., 2013). Evidence for differences in Middle and Late Holocene climate are therefore overall subtle when compared to the last glacial period, and long high-resolution paleoclimate records are necessary to measure and illustrate these changes. Very few studies from SWNA have produced highly resolved records of this period, but a climate transition from a warmer, drier Middle Holocene climate to a cooler and wetter Late Holocene climate has been reported in numerous studies using various proxies. A speleothem record of annual bands suggests that SWNA experienced an increase in effective moisture in the Late Holocene starting around 4000 yr BP based on stalagmite growth (Polyak and Asmerom, 2001), and a study of mites preserved in speleothems from SWNA by Polyak et al. (2001) suggests a wetter climate from 3200-800 yr BP. The majority of other climate records in SWNA come from packrat middens, lake records, and tree rings. Tree rings provide records of annual moisture in SWNA, however the longest record of precipitation only extends ~2000 yr BP (Grissino-Mayer et al., 1997). Evidence from lake levels in Estancia Basin found evidence for low groundwater during the Middle Holocene (7000-5400 yr BP) followed by a rise in the water table through the Late Holocene (Menking and Anderson, 2003). Persistent dry conditions throughout the Middle Holocene at Potato Lake in central

Arizona have also been recorded (Anderson, 1993), and arroyo cutting and filling in SWNA increased after 4000 yr BP as a result of wetter conditions (Waters and Haynes, 2001). A "midden gap" occurs in the packrat midden record from ~4 to ~9 ka (Betancourt et al.,1993) and two possible explanations are provided. It is suggested that there were either very dry winters and hot summers during the Middle Holocene that led to decreased midden production or increased monsoon precipitation and high humidity that would have hindered the crystallization of rat urine necessary for preservation of middens, which would argue for increased summer moisture during the Middle Holocene (Poore et al., 2005).

Elsewhere, Antevs (1955) defined the Middle Holocene in the Great Basin as significantly drier and referred to this period as the 'Altithermal' period, and since then climate studies such as Booth et al. (2005) present further evidence of a severe drought that affected mid-continental North America. A timberline study in the Sierra Nevada that suggests a warmer climate occurred from 6300-3500 yr BP (Scuderi, 1987) and a paleoflood study from the Mississippi River also suggests that during a drier period of 5000-3300 yr BP the flood maximums were less extreme than they were after 3300 yr BP when the climate became cooler and wetter (Knox, 1993). A continuous 8000-year record of temperature reconstructed from hydrogen isotopes in bristlecone pine tree rings from the White Mountains of California also suggests a general cooling trend from 6800 to 2000 yr BP (Feng and Epstein, 1994), which supports a timberline record from the area that shows declining treelines from 7400 to 200 yr BP (LaMarche, 1973).

This transition to cooler and wetter conditions corresponds with a shift from high Northern Hemisphere solar insolation during the Middle Holocene, known as the

Holocene Thermal Maximum, to decreased solar insolation during the Late Holocene (Renssen et al., 2012; Wanner et al., 2008; Berger and Loutre, 1991). Monsoon strength is positively correlated with solar intensity, and some evidence and models show that Northern Hemisphere monsoon strength, including the NAM, was greatest during the Middle Holocene (Metcalfe et al., 2015; Poore et al., 2005; Jiang et al., 2006). Higher insolation and a strengthened monsoon should have delivered more effective moisture to SWNA, but also resulted in higher temperatures (Feng and Epstein, 1994). It was followed by a relative decrease in monsoon strength and cooler temperatures, yet many of these records suggest an overall increase in effective moisture during the Late Holocene. This is unexpected given that summer monsoon moisture is the largest component of the annual moisture budget (Adams and Comrie, 1997).

Globally a definable climate transition has been established around 4.2 ka, formally subdividing the Middle and Late Holocene based on various proxy datasets (Walker et al., 2012), however, very few climate records from SWNA have the resolution to delineate these changes. This study aims to examine the Late Holocene 'greening' of SWNA, determine whether or not the 4.2 ka climate event is observed in the speleothem record, and discuss the potential climate forcings associated with the Middle and Late Holocene.

2.7 Climate forcing mechanisms

Variations in solar insolation correlate well with climatic changes (Asmerom et al., 2007), although the change in solar insolation forcing of climate itself is reportedly relatively small and should not directly account for the magnitude of change observed in climate records (Morely et al., 2014). In contrast, large changes in the UV flux in the upper atmosphere are observed and may help drive atmosphere-ocean coupled climate variability (Graham, 2004; He and Guan, 2013; Scaife et al., 2013). Variations in these climate patterns are likely to impact the strength and balance of both winter and summer precipitation in SWNA.

El Niño Southern Oscillation (ENSO) is one pattern that is a naturally occurring phenomenon characterized by fluctuations in temperature between the atmosphere and ocean in the tropical Pacific with a frequency of roughly every 2-8 years (Cole and Cook, 1998). Southern Oscillation refers to the seesaw-like atmospheric pressure differences between eastern and western tropical Pacific. There are two extreme phases of ENSO, El Niño and La Niña, each of which causes extreme weather in certain regions of the world. Because this is a Pacific phenomenon it primarily its effect is strongest on winter moisture in SWNA. During an El Niño event changes in atmospheric pressure gradients result in weakened trade winds and anomalously warm sea surface temperatures (SSTs) in the eastern and tropical Pacific Ocean. This reflects reduced strength of the Walker circulation, the east-west convective cycle that originates due to the SSTs along the equatorial Pacific. During El Niño years the storm track tends to shift farther south making winters wetter and cooler in SWNA. La Niña conditions involve strengthened trade winds (strengthened Walker circulation) and subsequently cooler SSTs along the equator and western coast of South America due to stronger upwelling. During La Niña years the storm track tends to shift farther north and SWNA receives less winter precipitation than normal (Metcalfe et al., 2015; Cook et al., 2007). ENSO may not have a significant effect on long-term effective moisture; however, if El Niño or La Niña are locked in a persistent pattern at the millennial scale, it could play an important role.

Another climate pattern, Pacific Decadal Oscillation (PDO), is a north Pacific phenomenon similar in character to ENSO in that it has a warm and cool phase that affects atmospheric winds, but it has a longer periodicity (15-30 years) than ENSO (Gray et al., 2003; Minobe, 1997). It is indexed by North Pacific SST anomalies, where the warm/positive phase tends to correlate with wetter winter conditions in SWNA (Asmerom et al., 2013; Metcalfe et al., 2015). Winter precipitation is especially important for groundwater recharge (Sheppard et al., 2002). Thus, it is likely that a shift in the amount of winter precipitation and groundwater recharge is related to changes in the strength and duration of ENSO and PDO phases (Menking and Anderson, 2003; Rasmussen et al., 2006).

Overall, as the insolation forcing in the Northern Hemisphere lessened in the Late Holocene, other forcings such as these described above likely became more influential on the NAM (Knudsen et al., 2011; Metcalfe et al., 2015) and overall climate of SWNA. It is possible that stalagmites may respond to seasonal moisture and represent seasonal changes rather than annual changes in effective moisture. However, the drip study in Carlsbad Cavern (Rasmussen, 2006) and observations of cave conditions over the last three decades favor that stalagmites in these caves preserve a record of annual effective moisture. For example, caves in the Guadalupe Mountains were wet with much active dripping and filled small pool basins during the 1980s when annual rainfall was greater, and with the onset of drought conditions beginning in 1991 the caves dried up significantly (V. Polyak, personal communication).

CHAPTER 3 METHODS

This study is based on uranium (U)-series dating of three stalagmites and respective analysis of climate proxy data within each sample. Stable isotope ($\delta^{18}O$ and $\delta^{13}C$), grayscale, $\delta^{234}U$, and trace element (Sr and Ba) data have been obtained for sample PD3. Stalagmite growth, grayscale, and stable isotope data have also been obtained for samples X2 and X3, both at a higher resolution than PD3 and similar resolution to one another. An ultra high resolution ~100-year section of X3 is also provided for proxy comparison that includes annual banding. Time-series for each set of data were constructed for comparison in order to establish climate proxies that relate to the difference in climate between the Middle and Late Holocene.

3.1 U-series dating

U-series dating works by utilizing the decay chain of Uranium-238 (Eq. 3.1).

$$^{238}U \rightarrow \ ^{234}Th \ \rightarrow \ ^{234}U \ \rightarrow \ ^{230}Th \qquad (3.1)$$

The half-life of ^{230}Th is 75,584 years (Cheng et al., 2013), which enables us to date materials up to about 650,000 years old, after which secular equilibrium is effectively reached. At secular equilibrium,

$$\lambda_1 N_1 = \lambda_2 N_2 \qquad (3.2)$$

where λ_1 is the decay constant of the parent and N_1 is the number of atoms of the parent nuclide, and λ_2 is the decay constant of the daughter and N_2 is the number of atoms of the daughter nuclide.

U-series dating is an ideal method for determining the age of carbonate rocks because when in its oxidized state as U^{6+}, which occurs easily on the surface environment, is very soluble and mobile, and Th has one oxidation state as Th^{4+} and is not soluble. Thus, groundwater and surface water are enriched in uranium compared to thorium, and when carbonate minerals precipitate from cave drip water they typically have sufficiently high uranium concentrations and very low to essentially no thorium and therefore no initial ^{230}Th. ^{230}Th present in the sample is (1) ^{230}Th produced from radioactive decay of ^{234}U and ^{238}U and (2) ^{230}Th inherited with detrital ^{232}Th, where the initial ^{230}Th /^{232}Th atomic ratio is typically assumed to be 4.4 x 10^{-6}, based on the assumption that the contaminant has a bulk silicate earth ^{232}Th/^{238}U (κ-value) of 3.8. Assuming secular equilibrium between ^{230}Th and ^{238}U gives a ^{230}Th/^{232}Th atomic ratio of 4.4 x 10^{-6}, detailed below in Equations 3.3 and 3.4.

$$\frac{^{232}Th}{^{238}U} = 3.8 \cdot \frac{\lambda_{230}}{\lambda_{238}} \tag{3.3}$$

$$\frac{^{230}Th}{^{232}Th} = \frac{\lambda_{238}}{\lambda_{230} \cdot 3.8} = 4.4\times10^{-6} \tag{3.4}$$

This initial value, however, is not applicable for Guadalupe Mountains stalagmites because the contaminant has a strong carbonate component, and a non-linear equation has been constructed and used to correct U-series ages of these stalagmites (Rasmussen, 2006). Thus, if the sample is pure and the system remains closed we can acquire dates from the isotope ratios as described in Equation 3.5 where the ^{230}Th /^{238}U ratio is measured and the decay constants are known. This technique allows for direct measurement of accurate and precise dates and is used to construct high-resolution chronologies for three speleothems in this study.

$$\left(\frac{^{230}Th}{^{238}U}\right) = \left(1 - e^{-\lambda 230 t}\right) + \left(\frac{\delta^{234}U}{1000}\right)\left(\frac{\lambda_{230}}{\lambda_{230}-\lambda_{234}}\right)\left(1 - e^{(\lambda 234 - \lambda 230 t)}\right) \tag{3.5}$$

Calcite subsamples of ~100 mg were drilled from stalagmite samples. The powders were weighed, transferred, and dissolved in 15N HNO_3. They were spiked with approximately 1 gram of mixed synthetic isotopes ^{229}Th-^{233}U-^{236}U, and were fluxed on a hot plate for 30 minutes. One drop of $HClO_4$ was added to dissolve any organic matter and then samples were dried down. Samples were brought up in 7N HNO_3 and Th and U were isolated in 2 mL anion exchange columns using Eichrom 1x8, 200-400 mesh chloride form resin; samples were flushed (cleaned) with 7N HNO_3 then Th was collected using 6N HCl and U was collected using H_2O and and 1N HBr. Th and U were dried down and dissolved in 3% HNO_3 to be analyzed separately using the Thermo NEPTUNE multi-collector inductively coupled plasma mass spectrometer (MC-ICP-MS) at the University of New Mexico Radiogenic Isotope Lab.

The instrument is equipped with switchable Faraday cup resistors with four 10^{12} Ω resistors, five 10^{11} Ω resistors, one 10^{10} Ω resistor and secondary electron multiplier (SEM). The SEM or Faraday cup with a 10^{12} Ω resistor in the center position can be used interchangeably to measure the least abundant isotope (^{234}U or ^{230}Th) depending on the strength of the signal (Asmerom et al. 2006). Signals of 5mV or less are measured using the SEM detector. When the SEM is used, a gain must also be measured throughout the duration of sample measurements in order to calibrate the SEM results to the Faraday cup measurements. Resistor settings of 10^{10} Ω are set for larger signals up to 500 volts used for the ^{238}U and in some cases the ^{232}Th signal, 10^{11} Ω for less than 50 volt signals, and 10^{12} Ω for less than 5 volt signals. The NEPTUNE is coupled to the Aridus II desolvating nebulizer that increases the signal by 4 times and reduces the necessary sample size by half, ultimately increasing efficiency by 8 times. The U standard NBL-112 and Th in-house standard were used to establish the efficiency control between the SEM and Faraday cups. Procedural blanks are ~10 pg and ~30 pg for Th and U, respectively.

Complete U-series chronologies were measured for stalagmites X2, X3, and PD3, and a high-resolution $\delta^{234}U$ time-series was constructed for stalagmite PD3.

3.2 Stable Isotope Analysis

Stable isotope data for speleothems in this study have been obtained from Matthew Lachniet at the Las Vegas Isotope Science Lab at the University of Nevada Las Vegas. Powders were drilled every 0.5 mm, 1 mm, and 2 mm for analysis on samples X2, X3, and PD3, respectively, using a 0.015” diameter drill bit. This provided a stable isotope measurement approximately every 4 years for both X2 and X3, and every 40 years for PD3. Stable isotopes are expressed in delta notation ($\delta^{18}O$ and $\delta^{13}C$) relative to the Vienna Pee Dee Belemnite (V-PDB) standard as defined by equation 3.6.

$$\delta^{18}O = \left(\frac{\frac{^{18}O}{^{16}O}_{sample} - \frac{^{18}O}{^{16}O}_{VPDB}}{\frac{^{18}O}{^{16}O}_{VPDB}} \right) \times 1000 \tag{3.6}$$

3.3 Trace Element Analysis

Powders of ~10 mg were milled every 2 mm along the growth axis of stalagmite PD3, diluted in 3% ultrapure HNO_3, and spiked to 10 ppb In (internal standard). Samples were then measured for Mg, Ca, Sr, Ba, and U on a Thermo X-Series II Quadrupole ICP-MS using multiple-element standards. Calibrations were performed approximately every twenty sample runs. Analytical uncertainties are generally <2% standard errors and reported as 1σ absolute errors. Concentrations were determined using dilution factors for each sample, and these match trace element ratios divided by Ca concentrations (e.g. Mg/Ca, Sr/Ca, Ba/Ca).

3.4 $\delta^{234}U$

Small powders (~10 mg) were milled along the growth axis of stalagmite PD3 every 2 mm to construct a high-resolution $\delta^{234}U$ time-series comparable with the elemental and stable isotope time-series. These powders were dissolved and processed in the anion resin columns described above in Section 3.1 for U-series analyses, except they were not spiked. The ratio of $^{234}U/^{238}U$ is expressed as the per mil (‰) amount (Eq. 3.7), and measured values were converted to initial $\delta^{234}U$ using the U-series chronology for each distance from the stalagmite top using Equation 3.8.

$$\delta^{234}U = \left[\frac{\left(\frac{^{234}U}{^{238}U}\right)}{\left(\frac{\lambda_{238}}{\lambda_{234}}\right)} - 1\right] \times 1000 \tag{3.7}$$

$$\delta^{234}U_i = \delta^{234}U_m \times e^{\lambda_{234}t} \tag{3.8}$$

3.5 Grayscale Analysis

Grayscale was measured for samples PD3, X2, and X3 by taking high-resolution images of thin sections using a slide scanner and splicing them together to produce a high-resolution grayscale stratigraphic record. The images were converted from bluescale to grayscale using Digital Micrograph, a digital image-processing program used primarily for electron microscopy. A multiple pixel transect through the growth axis and close to the stable isotope transect was analyzed for grayscale values over the length of the samples. The gray values were measured from thin sections. Grayscale values are assigned from 0 to 250 (black to white), where lower values therefore indicate dark layers and higher values indicate light layers in the transmitted light through the sections. Values for these speleothems range from 13 to 216 and the resolution is sub-annual. Grayscale appears to respond to rainfall amount or drip water availability, however, processes that control darkness of calcite layers are complex and variability in the apparent darkness of a speleothem can be misinterpreted for a number of reasons including potential differences in thin section thickness. Grayscale data in this study is therefore primarily used for spectral and wavelet analyses.

3.6 Annual Growth Bands

The types of speleothems used in this study show annual growth banding that are demonstrated by comparison with U-series age measurements along the same transect. Growth band thickness has been shown to be a proxy for rainfall amount in the study area, as speleothem growth is directly related to drip water availability. Thinner bands result from decreased rainfall and thicker bands from increase rainfall (Polyak and Asmerom, 2001; Asmerom et al., 2013). The banding is formed because of the seasonal variations in precipitation amount. The banding was primarily measured from thin sections using an optical microscope and Digital Micrograph.

3.7 Spectral Analysis

The REDFIT program works as an effective preliminary analysis of the different proxy time-series for paleoclimate records because it allows for spectral analysis from unevenly spaced time-series without needing to interpolate data. Spectral analysis enables the identification and strength of periodicities in a time-series (ie. seasonal, annual, 11-year sunspot, precession, etc.) by using a first-order autoregressive (AR1) process to estimate a null-hypothesis of “red-noise” to test if peaks in a spectrum are significant (Schulz and Mudelsee, 2002). Significant frequencies were measured using REDFIT for each proxy time-series. Periodicities observed at the 90% confidence interval or greater are reported in this study.

3.8 Wavelet Analysis

Wavelet analysis is another means of identifying periodicities in a time-series that allows for the determination of the dominant modes of variability and also how those modes vary in time (Torrence and Compo, 1998), which was not demonstrated by spectral analysis. This technique requires an evenly spaced data set, so proxy time-series data were interpolated using a built-in Matlab function “interp1.” Wavelet analysis was conducted on the interpolated data sets in a Matlab script using a Morlet wavelet with a wavenumber of 6. The character of periodicities measured by REDFIT can be directly observed in wavelet analyses to determine where they occur in time.

CHAPTER 4 RESULTS

Multiple climate proxies have been used in this study for the purpose of producing both a high-resolution and low-resolution record of climate in SWNA from the Middle to Late Holocene. Age models for stalagmites PD3, X2, and X3 using U-Th disequilibrium methods were used to construct stable isotope, grayscale, trace element, and $\delta^{234}U$ time-series. Stalagmite PD3 provided the long-term continuous lower resolution record from the Middle Holocene through the transition between Middle and Late Holocene and into the Late Holocene. Stalagmites X2 and X3 provided a high-resolution segment of the Middle and Late Holocene, respectively.

4.1 Stalagmite PD3

Age Model

The U-Th chronology as well as petrographic observations shows that this stalagmite grew continuously but nonlinearly from about 6000-1900 yr BP; top and bottom U-series ages are 2063 ± 231 years and 6077 ± 193 years. A total of 24 calcite powders were drilled and collected along the stalagmite's growth axis and 21 results were used to construct the age model. The average error for all samples is ±235 years with individual errors ranging from ±166 to ±516 years. The chronology is composed of a 6-order polynomial equation fit to the corrected U-Th ages (Fig. 5). U-series data is in Table 1.

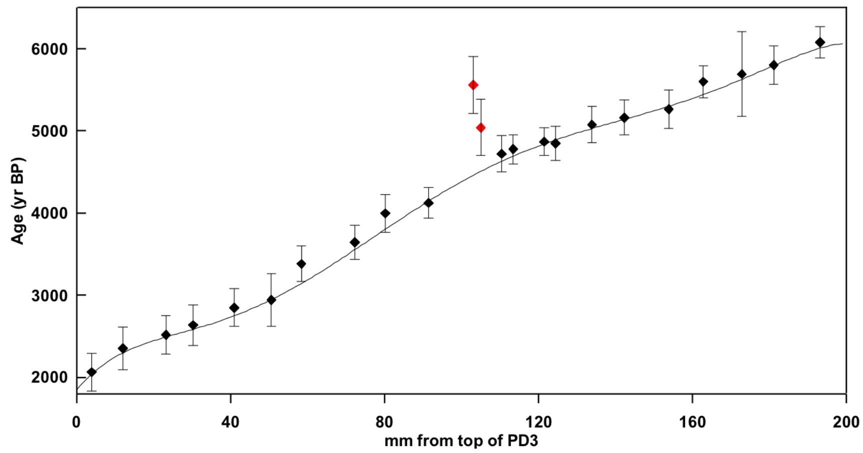

Figure 5 U-series age model for stalagmite PD3 constructed from 21 measured ages. 2σ errors are represented by the vertical bars. Polynomial equation defined in Eq. S1 in Appendix A.

Table 1 **U-series age data for stalagmite PD3.**

mm PD3	^{238}U ppb	^{232}Th pg/g	^{230}Th/^{232}T Activity	^{230}Th/^{238}U Activity	δ^{234}U Initial	δ^{234}U Meas	Age Uncorr	Age Corr
3.8	255±0.21	1902±48	18±0.511	0.0449±0.0005	760±1.8	755±1.8	2822±34	2063±231
12.1	377±0.26	5647±50	10±0.123	0.0512±0.0004	759±1.9	754±1.8	3223±26	2353±262
23.2	336±0.26	3574±46	15±0.228	0.0524±0.0004	759±1.8	754±1.8	3300±27	2516±236
30.2	295±0.22	3014±49	16±0.307	0.0550±0.0005	769±1.9	763±1.8	3451±31	2634±247
41	280±0.21	2332±44	21±0.439	0.0576±0.0005	771±1.8	765±1.8	3608±33	2848±230
50.1	264±0.17	4064±49	13±0.205	0.0639±0.0007	778±1.8	772±1.8	3995±44	2943±318
58.4	291±0.21	2197±44	26±0.565	0.0650±0.0005	769±1.8	762±1.8	4090±35	3379±216
72.2	271±0.24	1787±43	32±0.808	0.0690±0.0005	777±1.8	769±1.8	4328±32	3642±209
80.2	305±0.29	2736±49	26±0.487	0.0755±0.0005	777±1.9	769±1.8	4745±32	3995±227
91.4	305±0.25	1744±41	40±0.986	0.0755±0.0006	786±1.8	777±1.8	4723±36	4122±184
110.4	298±0.24	2543±39	31±0.504	0.0871±0.0005	789±1.9	779±1.8	5455±32	4720±223
113.4	594±0.47	6964±39	23±0.144	0.0867±0.0003	809±1.9	798±1.8	5370±19	1775±179
121.5	478±0.58	3706±40	34±0.404	0.0871±0.0004	803±1.9	792±1.8	5415±26	1868±166
124.4	347±0.27	3121±39	30±0.402	0.0893±0.0004	809±1.9	799±1.8	5536±28	4846±209
133.9	298±0.23	2529±45	33±0.630	0.0926±0.0006	789±1.9	777±1.8	5809±36	5075±223
142.3	263±0.20	1740±46	43±1.174	0.0935±0.0006	793±1.9	782±1.8	5852±41	5159±212
153.8	319±0.27	3209±53	29±0.536	0.0967±0.0007	802±1.9	791±1.8	6028±47	5264±234
162.8	260±0.24	1287±42	61±2.065	0.0991±0.0010	799±1.9	787±1.8	6200±62	5597±192
172.8	292±0.25	15968±53	7±0.045	0.1179±0.0007	799±1.9	786±1.8	7411±47	5690±516
181.1	245±0.23	1925±50	41±1.132	0.1063±0.0009	824±1.9	810±1.8	6568±55	5799±238
193.1	286±0.22	1672±43	56±1.480	0.1070±0.0007	801±1.9	787±1.8	6699±48	6077±193

Stable Isotopes, Trace Element, Transmitted Grayscale, and δ^{234}U Time-series

Stable isotopes in speleothems are understood to be important recorders of hydrologic processes and variability (McDermott, 2004; Lachniet, 2009) that provide information about relative temperature and moisture amount in the environment during growth.

$\delta^{18}O$

Modern spatial variations in δ^{18}O of precipitation are well characterized and are a function of several factors including distance from the source (ocean), altitude, latitude, temperature, and amount of precipitation (McDermott, 2004). Cave drip water and therefore speleothems from which they form are products of the local moisture, so the isotope values in the calcite reflect the local precipitation values. However, there are several processes that take place leading up to speleothem formation that can further affect isotope values. They give indications of a variety of environmental processes and features including the moisture source, temperature, amount effect, and temperature effect (Lachniet, 2009). Summer monsoon gulf moisture and Pacific moisture have distinctly different oxygen isotopic compositions over the study area. Summer NAM precipitation δ^{18}O values are around -3‰, which is significantly heavier than Pacific-derived moisture that has values around -11‰ (Asmerom et al., 2010). Because speleothems are a product of the groundwater from which they precipitate, they will primarily reflect the isotope values of the respective moisture source. In the case of SWNA, heavier calcite values in speleothems indicate a more dominant summer monsoonal moisture and lighter values indicate a more dominant Pacific-derived winter moisture in the absence of kinetic fractionation effects. Secondly, oxygen isotopes give an indication of temperature because fractionation in isotopic equilibrium conditions is increased with colder temperatures. Air temperatures at mid-latitude sites affect the $\delta^{18}O$ value of precipitation by about 0.5-0.69‰ $°C^{-1}$ but also affect calcite precipitation by affecting the cave air temperature, which results in about -0.24‰ $°C^{-1}$ in oxygen fractionation. The net result of this temperature affect is 0.25-0.35‰ $°C^{-1}$ in speleothems that formed in or near isotopic equilibrium, such as Fort Stanton Cave (Asmerom et al., 2010), north of the study area. Lighter isotopes are therefore expected in the calcite from cooler temperatures and heavier isotopes are expected from warmer temperatures (Lachniet, 2009). Additionally, the amount of rainfall can change isotope values in speleothems. Knowing that the heavy isotope is preferentially condensed and precipitated out first, we would expect the heavy isotope to be the product of precipitation. However, if all of the moisture is precipitated from a cloud, both the heavy and light isotope would be released and this would drive $\delta^{18}O$ values in the rain lighter than would be otherwise expected, a result known as the amount or rainout effect (Sharp, 2007). Evaporation also takes place on the surface and in the caves, which evaporates the light isotope preferentially and leaves the heavier isotope to be crystallized in the calcite. All of these processes and effects shape the values preserved in stalagmites.

$\delta^{13}C$

$\delta^{13}C$ data tend to reflect local productivity (vegetation amount and type), which is ultimately related to the effective moisture. Carbon isotopes in speleothems reflect the soil CO_2 composition, which indicates the type of plant system (C3 or C4) present during the time of growth (McDermott, 2004; Lachniet, 2009). The different photosynthetic pathways between C3 and C4 plants result in significant fractionation differences. C3 plant systems represent the majority of plants in the world and are indicative of an environment with ample water availability. $\delta^{13}C$ values for C3 plants are very light and range from -23‰ to -33‰ (Sharp, 2007). Conversely, C4 plants grow in arid regions and represent moisture-limited environments. They show less isotopic fractionation than C3 plants and have significantly heavier $\delta^{13}C$ values ranging from -9‰ to -16‰ (Sharp, 2007). Knowing the type of plant system present during speleothem growth therefore gives valuable information about the amount of effective moisture at the time of formation.

In addition to organic matter as a carbon source for speleothems, limestone bedrock contributes a heavy $\delta^{13}C$ signal (3‰ to 8‰) (Hill, 1987). During dry periods, water has a longer residence time in the ground and therefore has more time to pick up a larger bedrock carbon signal, driving the values heavier. During wet periods, water flows through the bedrock readily and does not pick up as much carbon from the bedrock, driving values lighter. Like oxygen isotopes, evaporative environments kinetically fractionate carbon and therefore aridity will result in heavier $\delta^{13}C$ values.

Covariance in $\delta^{13}C$ and $\delta^{18}O$

Given that the samples used in this study come from evaporative cave environments, it is expected that more evaporation results in more kinetic fractionation, a process that drives both the carbon and oxygen isotopes of the precipitated calcite to heavier values as a result of different masses experiencing different translational velocities during a phase change (Sharp, 2007). Kinetic fractionation tends to occur where cave relative humidity is low; therefore, carbon and oxygen isotope ratios tend to co-vary and change linearly in well-ventilated caves in semi-arid areas such as Pink Dragon Cave and Christmas Tree Cave.

$\delta^{18}O$ and $\delta^{13}C$ measured values for stalagmite PD3 are in Table S1 (in appendix). The average $\delta^{13}C$ value is -5.2‰ and the average $\delta^{18}O$ value is -3.7‰. Both carbon and oxygen time-series exhibit decadal to centennial-scale variability, but do not demonstrate a distinct transition between Middle and Late Holocene climate (Fig. 6), although there are periods of elevated values for the $\delta^{18}O$ between 6000 and 5000 yr BP.

Strontium and barium trace element data for stalagmite PD3 are used in this study for providing a continuous record through the Middle to Late Holocene transition. Concentrations of trace elements such as strontium and barium in precipitated carbonate minerals reflect the chemical composition of drip water and the physical conditions present at the time of formation. Trace element concentrations in speleothems are therefore understood to be paleoclimate indicators that are controlled by rates of evaporation and degassing as well as changes in water residence time and the degree of water-rock interaction (Fairchild et al., 2000; Fairchild and Treble, 2009; Tremaine and Froelich, 2013; Banner, 1995; Railsback et al., 1994). In semi-arid locations such as the Guadalupe Mountain caves it is suggested that trace element variations in speleothems are predominantly driven by evaporative concentrations of drip waters. Evaporative conditions increase the concentration of ions in solution, which causes greater ionic strength and supersaturation relative to calcite. This results in higher concentrations during more arid periods and lower concentrations during wetter periods (Railsback et al., 1994). Trace element data are in Table S2. Sr and Ba show higher concentrations in the

Middle Holocene and a distinct shift from higher concentrations to lower concentrations around 4200 yr BP (Fig. 6).

The decay of ^{238}U to ^{234}U occurs by an intermediate step to ^{234}Th but involves decay by an alpha particle that results in damage of the crystal lattice site that ^{234}U occupies. When alpha particle emission occurs in limestone, this calcite/dolomite lattice weakening makes ^{234}U susceptible to leaching into water that is infiltrating through the bedrock. Secondary minerals such as such as calcite and aragonite that make up speleothem carbonate are thus typically enriched in ^{234}U in semi-arid regions. The ratio of $^{234}U/^{238}U$ is therefore another proxy used to describe variations in effective moisture (Ayalon et al., 1999, Zhou et al, 2005, Polyak et al., 2012). $\delta^{234}U$ values tend to be higher during drier periods when water moves more slowly through the bedrock, leaching more ^{234}U along the way. $\delta^{234}U$ values thus tend to be lower during wetter periods when water is more readily flushed through the bedrock. $\delta^{234}U$ measured values are in Table S3. A total of 84 subsamples were used to produce the $\delta^{234}U$ time-series. The record shows an overall decrease in values from the Middle to the Late Holocene (Fig. 6) with a distinct decrease at 4200 and 3800 yr BP.

Grayscale data is in Table S4. The grayscale time-series constructed from transmitted light of thin sections has a sub-annual resolution and shows greater variability during the Late Holocene beginning around 4000 yr BP. (Fig. 6).

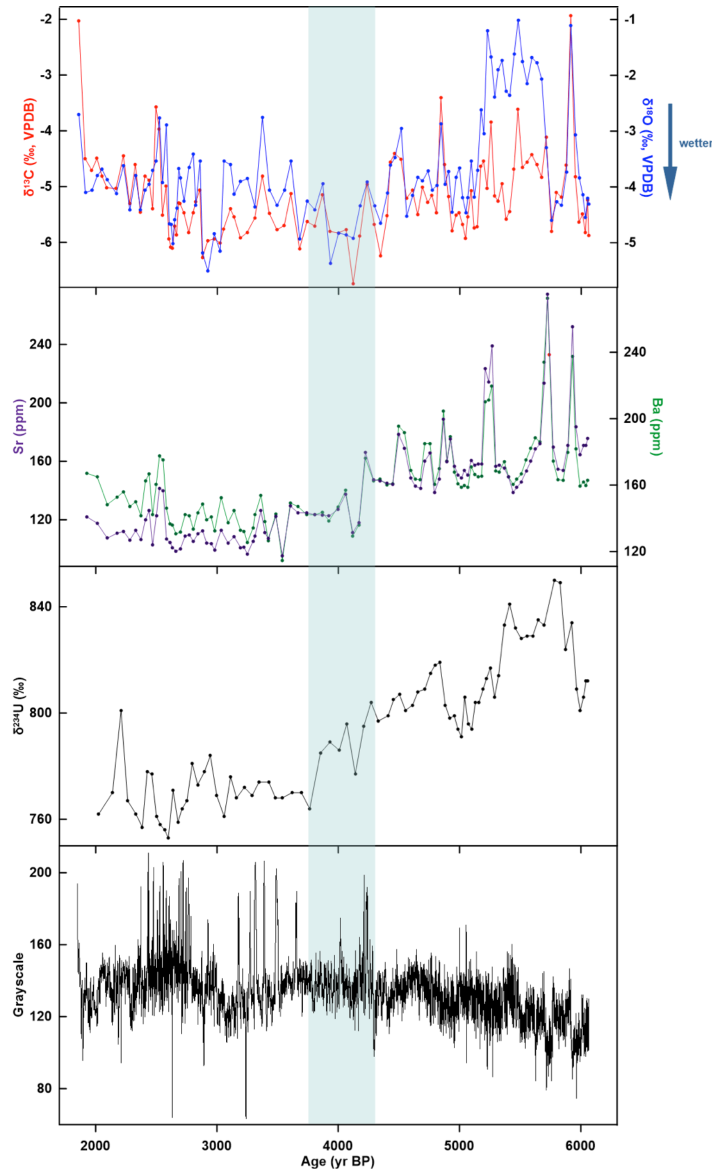

Figure 6 Stalagmite PD3 proxy time-series records. From top to bottom- carbon and oxygen stable isotopes, Sr and Ba, $\delta^{234}U$, and grayscale. Blue rectangle overlaps proposed 4.2 ka transition period.

Spectral and Wavelet Analyses

Significant periodicities (above the noise level at the 90% confidence interval) produced by spectral analysis of these proxies using REDFIT are in Table 4. Wavelet analysis results for grayscale data from stalagmite PD3 are shown in Figure 7. Significant decadal periodicities (between 10 and 30 years) were measured and are more prominent over the last ~4000 years.

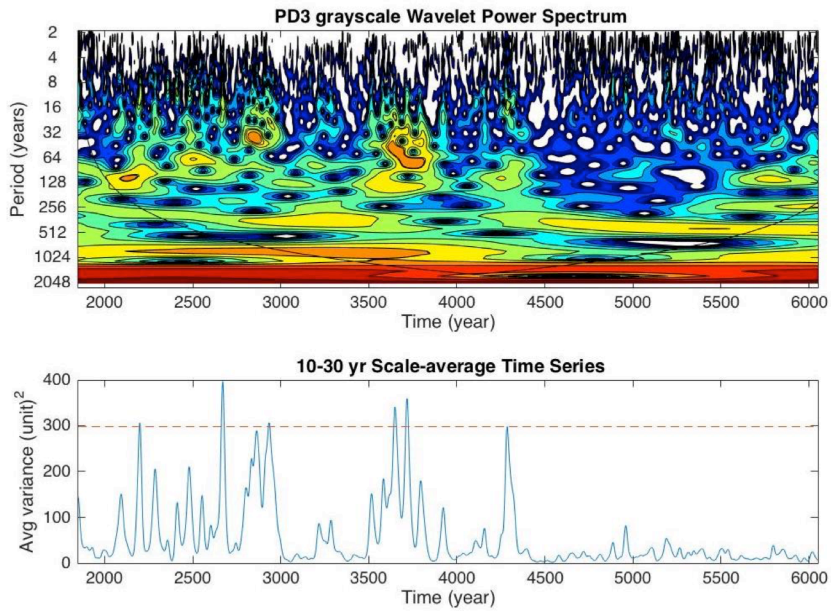

Figure 7 Wavelet analysis of stalagmite PD3 grayscale data. Spectral power is indicated by colors from blue (weak) to red (strong). Solid black line indicates 95% confidence interval (power significance). The 10-30 yr scale-average indicates PDO-like periodicities. There is increased decadal variability during the Late Holocene beginning around 4200 yr BP.

4.2 Stalagmites X2 and X3

Age Model X2

Stalagmite X2 represents a high-resolution segment of the latter part of the Middle Holocene. Stalagmite X2 grew continuously but nonlinearly from about 6500-4000 yr BP; top and bottom U-series ages are 4155 ± 87 years and 6363 ± 100 years. A total of 13 calcite powders were collected along the stalagmite's growth axis and used to produce a chronology composed of three polynomial age equations (Fig 8). The average error for all samples is ±113 with individual errors ranging from ±54 to ±384. U-series age data for stalagmite X2 is in Table 2.

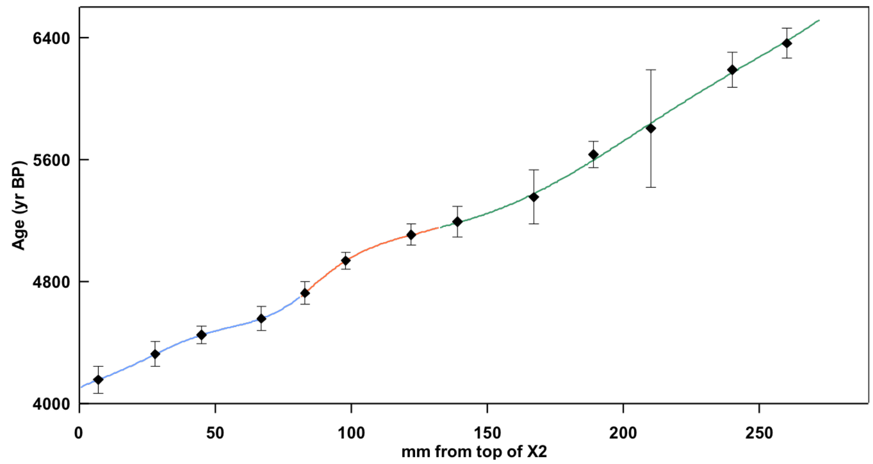

Figure 8 U-series age model for stalagmite X2. 2σ errors are represented by the vertical bars. Three polynomial equations defined in Eq. S2 in Appendix A.

Table 2 **U-series age data for stalagmite X2.**

mm X-2	**^{238}U ppb**	**^{232}Th pg/g**	**^{230}Th/^{232}Th Activity**	**^{230}Th/^{238}U Activity**	**δ^{234}U Initial**	**δ^{234}U Meas**	**Age Uncorr**	**Age Corr**
7	722±0.81	2692±43	78.2±1.3	0.0954±0.0003	1461±2.5	1444±2.4	4326±13	4155±87
28	792±1.15	3003±32	81±0.9	0.1006±0.0003	1508±2.5	1489±2.5	4482±13	4323±81
45	590±0.62	383±37	456±44	0.0970±0.0003	1376±2.4	1358±2.4	4562±14	4449±59
67	591±3.05	839±28	215±7.1	0.1000±0.0006	1376±5.8	1358±5.7	4704±29	4557±79
83	501±0.55	587±25	280±12	0.1073±0.0003	1465±2.5	1445±2.4	4874±14	4725±76
98	560±0.45	219±34	841±131	0.1075±0.0003	1392±2.4	1372±2.4	5034±15	4936±54
122	494±0.46	396±38	441±42	0.1158±0.0003	1481±2.5	1459±2.5	5237±16	5106±69
139	410±0.51	653±35	218±12	0.1138±0.0004	1370±2.4	1350±2.3	5387±18	5191±100
167	324±0.30	1537±34	72.3±1.6	0.1123±0.0004	1212±2.2	1192±2.2	5707±21	5353±178
189	406±0.51	317±36	452±51	0.1154±0.0004	1239±2.3	1219±2.2	5797±20	5633±86
210	313±0.41	11592±59	10.0±0.1	0.1207±0.0006	1075±2.2	1055±2.2	6569±34	5803±384
240	634±0.69	3262±46	77.0±1.1	0.1296±0.0004	1280±2.3	1257±2.3	6414±19	6189±114
260	424±0.39	470±45	337±32	0.1223±0.0004	1107±2.1	1087±2.1	6554±23	6363±100

Age Model X3

Stalagmite X3 grew continuously from 1946-1024 yr BP; top and bottom U-series ages are 999±105 and 1853±147. An age model was produced using three polynomial age equations (Fig. 9). The average error for all samples is ±88 with individual errors ranging from ±49 to ±147. U-series age data for stalagmite X3 is in Table 3.

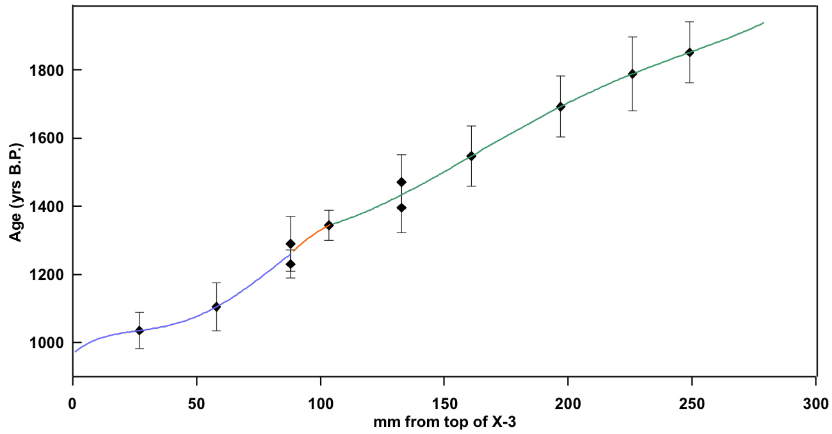

Figure 9 U-series age model for stalagmite X3. 2σ errors are represented by the vertical bars. Three polynomial equations defined by Eq. S3 in Appendix A.

Table 3 **U-series age data for stalagmite X3.**

mm X-3	^{238}U ppb	^{232}Th pg/g	^{230}Th/^{232}Th Activity	^{230}Th/^{238}U Activity	δ^{234}U Initial	δ^{234}U Meas	Age Uncorr	Age Corr
3.4a	855±6.56	2980±31	18.95±0.84	0.02±0.0009	1009±11	1006±11	1182±52	999±105
3.4b	848±5.87	2897±43	18.88±0.97	0.02±0.0010	1010±11	1008±11	1152±58	969±108
27	879±2.18	500±56	109.4±12.3	0.02±0.0003	972±4.7	970±4.7	1135±15	1035±53
58a	841±6.29	1665±23	34.96±1.81	0.02±0.0011	1029±13	1026±13	1226±63	1074±98
58b	837±5.44	1619±22	37.48±1.93	0.02±0.0012	1024±13	1021±13	1287±65	1135±100
88a	850±2.03	1700±49	39.84±1.20	0.03±0.0002	1032±1.1	1028±1.1	1410±13	1259±77
88b	892±2.18	3242±54	21.08±0.42	0.03±0.0003	964.9±5.4	961.6±5.4	1403±16	1218±49
104a	967±2.36	3359±78	24.33±0.63	0.03±0.0003	1032±1.4	1028±5.2	1496±17	1330±85
104b	949±2.30	2063±54	37.98±1.04	0.03±0.0002	1035±1.2	1031±1.2	1460±13	1316±73
104c	928±2.26	6600±87	13.12±0.25	0.03±0.0004	1028±2.0	1023±2.0	1657±23	1439±111
104d	879±2.11	4406±50	17.28±0.25	0.03±0.0003	1022±1.11	1018±1.06	1542±14	1340±102
133	918±2.27	1707±57	46.05±1.63	0.03±0.0003	1006±4.82	1002±4.80	1538±18	1395±73
161	829±3.94	1723±22	46.25±1.29	0.03±0.0007	1037±6.01	1032±5.98	1703±44	1547±89
197	1328±3.2	10703±75	13.25±0.13	0.03±0.0003	1063±4.17	1058±4.15	1868±14	1692±89
226	1123±2.7	11768±60	10.87±0.09	0.04±0.0003	1051±3.76	1046±3.72	2004±15	1788±109
249a	986±12.9	5753±50	20.07±0.56	0.04±0.0011	1071±16.9	1065±16.8	2043±63	1850±114
249b	983±8.95	5811±59	19.87±1.07	0.04±0.0021	1073±10.6	1067±10.6	2046±111	1853±147

Stable Isotope and Grayscale Time-series X2

δ^{18}O and δ^{13}C measured values for sample X2 are in Table S5. The mean δ^{13}C value for sample X2 is -5.2‰. δ^{13}C shows a ~7‰ variation through the record with values ranging from -8.2‰ to -1.0‰ (Fig. 10). It shows an excursion up to 2.4% at the end of the record around 4140 years B.P. associated with the top of the sample and termination of growth. The mean $\delta^{18}O$ value is -4.9‰. $\delta^{18}O$ shows approximately a 5‰ variation through the record with values ranging from -7.2‰ to -2.0‰ and also shows an excursion at 4140 years B.P. up to -1.0‰ (Fig. 10). Grayscale data constructed from transmitted light of thin sections is in Table S7.

Stable Isotope, Grayscale, and Growth Banding Time-series X3

$\delta^{13}C$ and $\delta^{18}O$ measured values for sample X-3 are in Table S6. The mean $\delta^{13}C$ value for sample X3 is -7.0‰, which is about 2‰ lower than sample X2. $\delta^{13}C$ shows approximately a 6‰ variation through the record with values ranging from -8.6‰ to -2.6‰ (Fig. 10). The mean $\delta^{18}O$ value is -6.1‰, which is about 1‰ lower than sample X2. The $\delta^{18}O$ record shows approximately a 5‰ variation through the record with values ranging from -8.0‰ to -2.9‰ (Fig. 10). Grayscale data is in Table S7. Annual growth band thickness was measured for sample X3 and values are in Table S8. Band thickness measurements range from 0.1 to 0.7 mm.

Correlation coefficients were measured for carbon versus oxygen in stalagmites X2 and X3. The Late Holocene shows slightly higher correlation with an $R^2 = 0.64$ than the Middle Holocene that has an $R^2 = 0.54$.

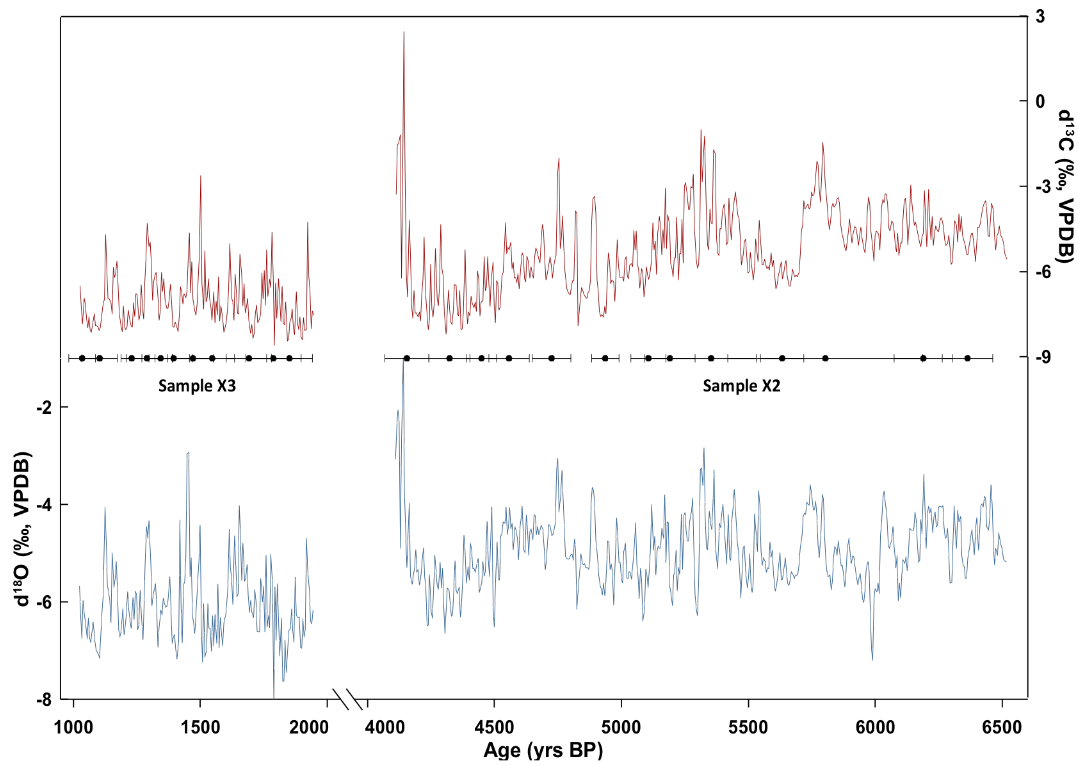

Figure 10 $\delta^{13}C$ and $\delta^{18}O$ time-series records for stalagmites X2 (Middle Holocene) and X3 (Late Holocene).

Spectral and Wavelet Analyses X2

Spectral analysis of $\delta^{13}C$ and $\delta^{18}O$ were determined using REDFIT. The measured periodicities and their confidence intervals are in Table 4. In addition to spectral analysis, the carbon and oxygen isotope and grayscale time-series were interpolated to 5-year resolution and analyzed using a continuous wavelet transform in Matlab to determine the timing of observed periodicities. Significant decadal periodicities (between 10 and 30 years) were measured to compare the Middle and Late Holocene decadal variance. $\delta^{13}C$ and $\delta^{18}O$ in sample X2 record effectively the same periodicities because of their strong covariation and thus show similar wavelet results. Overall, spectral and wavelet analyses results in the X2 proxies show that the decadal variance is very weak (Fig. 11).

Spectral and Wavelet Analyses X3

Spectral analysis of δ^{13}C and δ^{18}O, grayscale, and band thickness were determined using REDFIT. The measured periodicities and their confidence intervals are in Table 4. Measured frequencies range from 2 to 186 years.

The shorter frequencies (3-5 years) are detected in the growth banding data.

δ^{13}C and δ^{18}O data was interpolated to a 5-year resolution and wavelet analysis results of the carbon and oxygen isotope records for sample X3 show a strong decadal variation (Fig. 11).

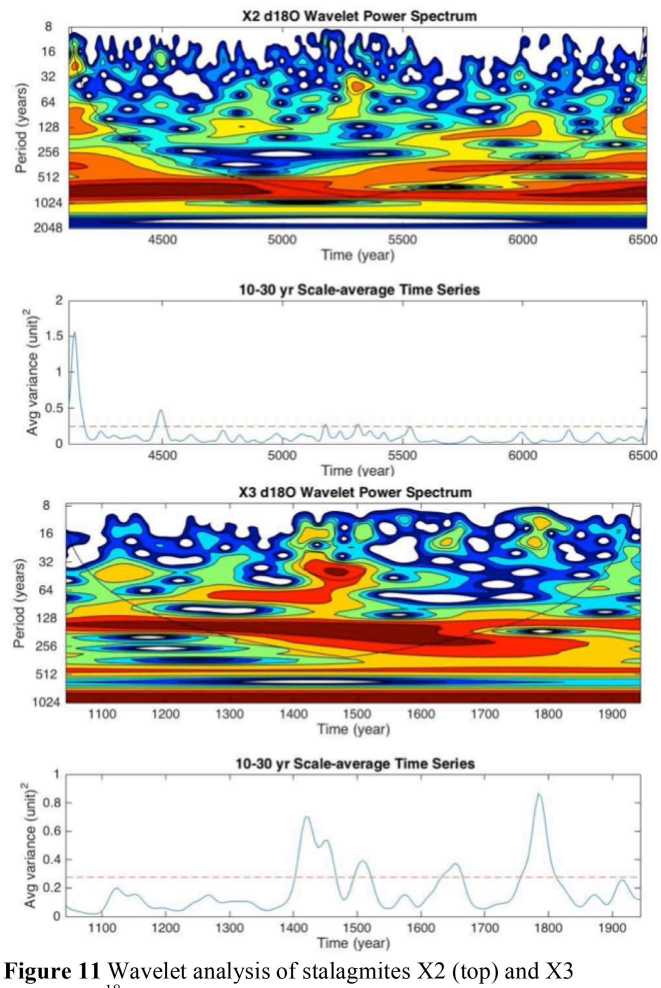

Figure 11 Wavelet analysis of stalagmites X2 (top) and X3 (bottom) δ^{18}O data. Spectral power is indicated by colors from blue (weak) to red (strong). Solid black line indicates 95% confidence interval (power significance). Significant 10-30 year periodicities were tested. X3 shows much greater PDO-like variability.

4.3 Stalagmite X3 Slide 9

High-resolution analysis of a 100-year period in thin section slide 9 of stalagmite X3 provides a comparison of speleothem proxies used in this study. This period was ~1400 yr BP. Carbon and oxygen stable isotopes grayscale, and growth band thickness were measured in this sample and spectral and wavelet analysis were performed. Grayscale values are inversely correlated with the stable isotope values. During periods when $\delta^{18}O$ and $\delta^{13}C$ are high it is interpreted as a more arid climate during which there is less water dripping into the cave, resulting darker speleothem layers in transmitted light. The darker layers produce lower grayscale values, which is the cause of the inverse relationship with $\delta^{18}O$ and $\delta^{13}C$. Spectral and wavelet results of this period show the same dominant frequencies (Table 4), which implies that these proxies are responding to similar mechanisms to record the same periodicities and can thus be used together to make climatic interpretations.

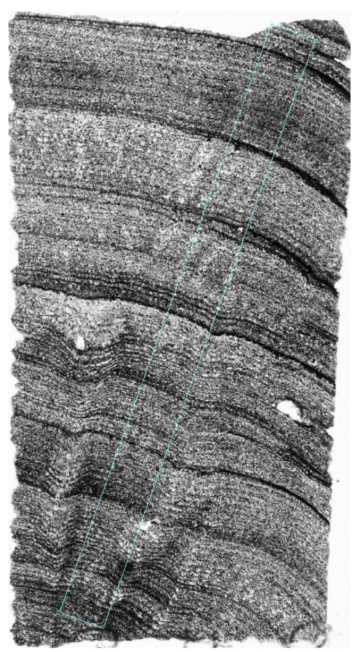

Figure 12 Scanned image of 3 slide 9 thin section.

Table 4 REDFIT spectral analysis results for $\delta^{13}C$ and $\delta^{18}O$, grayscale, and growth banding in stalagmites PD3, X2, and X3. Confidence interval percent values refer to the frequency above noise level. Reported values are in units of years.

Time-series	**99% confidence interval**	**95% confidence interval**	**90% confidence interval**
PD3 carbon	93, 212	81, 106	125, 157, 170
PD3 oxygen	93	85, 101, 115, 125, 212, 283	163, 353, 1060
PD3 Sr	-	123, 167, 245	208, 463
PD3 Ba	-	123, 167, 231	208, 463
PD3 $\delta^{234}U$	-	113, 185	-
PD3 gray	6, 7, 8, 10, 14, 15, 20, 33	11, 12, 13, 16, 18, 25, 28, 200	40
X2 carbon	9, 17, 18, 20, 25, 602	10, 11, 12, 13, 22, 402	10, 29, 69, 104
X2 oxygen	9, 16, 17, 19, 20, 25	11, 13, 17, 18, 22, 27, 402, 806	12, 23, 55, 71, 105, 121
X2 gray	11, 13, 17, 241	10, 11, 12, 13, 16, 18, 22, 30	13, 14, 16, 17, 20, 24, 89
X3 carbon	8, 154	7, 10, 17	11, 12, 15, 16, 42
X3 oxygen	8, 16, 154	7, 11, 42	9, 10, 15, 17
X3 grayscale	-	11, 13, 15	13, 16, 85, 186
X3 banding	3, 4, 5, 37, 155	2, 6, 9, 62	-
X3 slide 9 carbon	6, 9, 12	14, 18	-
X3 slide 9 oxygen	6, 11, 14	7, 8, 9, 18	-
X3 slide 9 gray	-	2, 3, 10	7, 12
X3 slide 9 bands	4	2, 3	10, 32

CHAPTER 5 DISCUSSION

Characterizing differences in the Middle versus Late Holocene climate by integrating multiple proxies is challenging due to disparities in temporal resolutions, climate sensitivities, and the extent that the chronologies are constrained (Barron and Anderson, 2011). These difficulties are evident in this study; partly due to the apparent subtle differences between these two periods; however, by establishing a continuous record that defines the climate transition from the Middle to Late Holocene by several independent proxies in one stalagmite we are able to constrain the timing and nature of the transition as well as the overall trend of the climate over this period. Additionally, by producing a record from two stalagmites of similar growth rate, climate sensitivity, chronological resolution, and proxy resolution, direct comparison of portions of the Middle and Late Holocene high-frequency climate variability can be made for SWNA.

5.1 Long-term climate transition

Trace element and $\delta^{234}U$ data from stalagmite PD3 show a subtle transition around 4200 yr BP from higher values to lower values. Trace element partitioning in speleothems is complex but it reflects hydrologic changes over time because it depends on the rates of CO_2 degassing and calcite precipitation (Fairchild and Treble, 2009). In evaporative settings such as caves in the Guadalupe Mountains it is therefore likely that trace element partitioning in speleothems is accentuated and reflects changes in the climate, where higher concentrations of Sr and Ba would indicate a warmer and more arid climate and lower concentrations would indicate a cooler and wetter climate. Similarly, variations in $\delta^{234}U$ values are interpreted to indicate residence time or infiltration rate of precipitation through soil and bedrock (Polyak et al., 2012), where more ^{234}U is picked up during drier periods when water flows more slowly through the bedrock. Based on these interpretations, higher trace element concentrations and $\delta^{234}U$ values that are observed during the Middle Holocene from ~6000 to ~4200 yr BP in stalagmite PD3 suggest it was slightly warmer and drier than the Late Holocene where values lowered around ~4000 yr BP. These results are similar to other speleothem records from SWNA that suggest the Middle Holocene climate was overall slightly warmer and drier than the Late Holocene, evidenced by the general lack of growth during the Middle Holocene until around ~4000 yr BP (Polyak and Asmerom, 2001). The trace element and $\delta^{234}U$ data further demonstrate that there was an observable shift in the climate around 4200 yr BP in SWNA, consistent with the timing of the Middle to Late Holocene transition observed in other global records (Walker et al., 2012).

Additionally, the grayscale record from stalagmite PD3 shows a slight increase in values overall (lightening of gray) from the Middle to Late Holocene, which indicates the climate became gradually wetter overall. The visual increase in variability observed in the grayscale time-series also suggests that the Late Holocene experienced greater climate variability than the Middle Holocene starting around 4000 yr BP, and the wavelet analysis results provide evidence that stronger interdecadal and decadal periodicities began around 4000 yr BP (Fig. 7). Increased variability in the Late Holocene is likely a result of increased ENSO/PDO activity that is evidenced to have begun around 4000 yr BP (Barron and Anderson, 2011; Conroy et al., 2008) and would suggest that a gain in effective moisture was due to the introduction of greater Pacific-derived winter precipitation.

While the stable isotope records do not show a clearly defined transition, they do show a dip in values and higher variability between ~4200-3800 yr BP. This period overlaps with a strong decadal variance observed in the grayscale wavelet analysis results, which we interpret as increased ENSO/PDO activity. The dip in values may suggest this was a cooler and wetter interval that could be the result of more frequent El Niño events and/or positive PDO phases during the period of global transition from Middle to Late Holocene. The stable isotope record also shows centennial-scale periodicities, and the dominant modes of centennial variability from spectral analysis are 93, 123, 167, 212, and 167 that indicate the climate of SWNA is in part modulated by fluxes in solar radiation (Asmerom et al., 2007; Ogurtsov et al., 2002; Sonett and Finney, 1990). However, sampling resolution of stable isotopes in stalagmite PD3 prevents the observations of frequencies below the 50-year interval, which prevents drawing conclusions about ENSO/PDO variability from the stable isotope time-series. The stable isotope values are effectively the same in the Middle Holocene as they are in the Late Holocene, suggesting the climate was overall similar.

Trace elements and $\delta^{234}U$ are hydrological indicators that record changes in residence time of groundwater, so it is likely that they are more sensitive to changes in subsurface hydrology than stable isotopes, which are affected more by cave and atmospheric air dynamics. If increased moisture observed in the Late Holocene is a result of increased winter precipitation, which is critical for groundwater recharge (Sheppard et al., 2002), trace elements and $\delta^{234}U$ might be more likely to record this signal and could account for the shift observed in their records that is not observed in the stable isotope records.

5.2 High resolution climate variability in the Middle and Late Holocene

In this study stalagmite X2 represents the Middle Holocene and stalagmite X3 represents the Late Holocene. They provide high-resolution records of climate variability during these periods because of their fast growth rates and sampling resolutions. Although the record is established from two different samples, their stable isotope values are comparable under the assumptions that they grew near each other in the same cave, have similar growth rates, and are measured at similar resolutions.

The $\delta^{13}C$ and $\delta^{18}O$ records produced from stalagmites X2 and X3 shows a simple observational trend somewhat congruent with the stalagmite PD3 record. In general the stable isotope values are 1-2‰ heavier during the Middle Holocene than the Late Holocene, which we interpret as slightly warmer and more arid conditions accompanied by a potentially greater summer monsoonal input. This interpretation corresponds with the decreasing strength of summer insolation from the Middle to Late Holocene where the NAM was at its peak around 6000 yr BP (Metcalfe et al., 2015). Increased summer insolation during the Middle Holocene would have increased the land surface temperature, giving more convective potential for monsoonal circulation. However, whether the Middle Holocene NAM was likely stronger (wetter), extended over a larger region geographically, or was simply the primary moisture source due to lack of winter precipitation is difficult to conclude from the data in this study. Higher temperatures strengthening the monsoon would also be accompanied by enhanced evaporation, lowering the effective moisture during the Middle Holocene. We interpret the lighter stable isotope values during the Late Holocene as cooler and wetter conditions with additional moisture from an increase in winter precipitation. Snowmelt from winter precipitation is an important contributor to groundwater supply, whereas much of the summer monsoonal precipitation evaporates before it infiltrates into groundwater reservoirs (Sheppard et al., 2002). Decreasing evaporation in response to dropping temperatures into the Late Holocene would have additionally reduced the impact of evaporation, resulting in an overall wetter climate.

This trend is consistent with the trace element and $\delta^{234}U$ records from stalagmite PD3. However, the growth periods of stalagmites X2 and X3 would suggest that the period from ~4000-2000 yr BP represents a growth hiatus and would indicate that conditions were not suitable for stalagmite growth, perhaps due to slightly more arid conditions. Alternatively, because only two samples were collected from this cave this may also be due to lack of sampling in Christmas Tree Cave. Powders drilled at tops and bottoms of broken segments of another stalagmite left on the cave floor shows growth of <2300 and greater than 2900 yr BP, which would fill in much of this ~4000-2000 yr BP gap. Overall, this record does show that the latter part of the Middle Holocene climate was similar to that of the Late Holocene and that overall differences are subtle.

Multicentury variability that is observed in the Middle Holocene record is almost completely absent from the Late Holocene record except for a 154-year periodicity. This likely reflects the 126-year solar signal that is also preserved in the Late Holocene speleothem record from stalagmite BC2 (Rasmussen et al., 2006) and was demonstrated to contribute to SWNA climate variability during the Holocene (Asmerom et al., 2007). Variations in the $\delta^{18}O$ record are visibly more frequent and more extreme during the Late Holocene, suggesting a more variable climate compared to the Middle Holocene. This is supported by the wavelet results that show a strong decadal frequency during the Late

Holocene that is not observed during the Middle Holocene (Fig. 11). Spectral analysis of this data also indicates a 2, 3, and 7-year periodicity present in the Late Holocene record that is not observed in the Middle Holocene record. These observations suggest the Late Holocene experienced increased PDO and ENSO-like variability, and are consistent with Rasmussen (2006) and Rasmussen et al. (2006) who suggested the Late Holocene climate is modulated strongly by PDO. The combined X2 and X3 record extends the high-resolution Late Holocene speleothem record established in Rasmussen (2006) into the Middle Holocene for comparison. Common behavior is observed in $\delta^{18}O$ data from stalagmite X3 and annual growth band data from stalagmite BC2 (Rasmussen et al., 2006) in which wavelet analysis demonstrates that both show significant decadal variability around ~1800 and between 1400-1600 yr BP, then relatively weak decadal variability after ~1400 yr BP.

A more active PDO would increase Pacific-derived precipitation during the winter in SWNA when in its positive phase and cause droughts in SWNA when in its negative phase. However, depending on its alignment with ENSO phases these effects can be enhanced or dampened (Wang et al., 2014). Frequent droughts and pluvial episodes have been observed in Late Holocene climate records (Kirby et al., 2015; Wang et al., 2014; Rasmussen et al., 2006; Cook et al., 2007; Woodhouse et al., 2009), and this high-frequency variability is attributed to increased ENSO/PDO activity. Even though brief drought episodes were likely more frequent in the Late Holocene, the pluvial episodes and overall cooler climate probably resulted in slightly greater overall effective moisture in the Late Holocene relative to the latter part of the Middle Holocene.

Strong correlation between carbon and oxygen isotopes is indicative of more evaporation (drier conditions), and though comparable for the two periods, correlation between carbon and oxygen in the Middle Holocene is lower than during the Late Holocene. This is unexpected under the interpretation that the Middle Holocene was more arid, and this finding suggests that it was not significantly drier than the Late Holocene. One explanation for the higher R^2 value in the Late Holocene could be the result of more frequent La Niña induced droughts that caused more periodic periods of evaporation to occur in the cave. The greater variability likely results in greater correlation of carbon versus oxygen isotope values, and may be caused by more frequent pluvial as well as drought episodes, with an overall slightly wetter average. Additionally, overall cooler temperatures in the Late Holocene would drive more ventilation in the caves, leading to more evaporation and higher correlation of carbon and oxygen isotope values.

5.3 Comparison to other climate proxies

Dongge cave in southeastern China receives the majority of its moisture from the East Asian monsoon (EAM) that is demonstrated to have weakened from the Middle to Late Holocene based on speleothem $\delta^{18}O$ data, lake sediment, and other climate proxies generally following the decrease in summer insolation (Chen et al., 2015; Wang et al., 2005) and its influence on land-sea temperature contrasts. $\delta^{234}U$ data from Dongge cave (Wang et al., 2005) shows increasing values from the Middle to the Late Holocene, which is opposite that of stalagmite PD3 (Fig. 13).

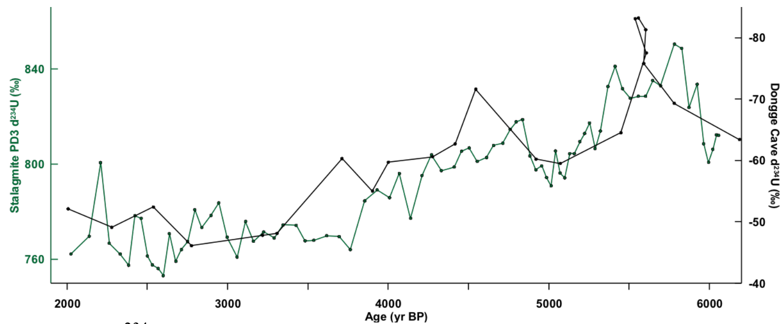

Figure 13 δ^{234}U from Dongge cave (inverted) (Wang et al., 2005) compared to stalagmite PD3.

The aridification observed in the δ^{234}U record from Dongge Cave is interpreted to directly represent the weakening of the EAM into the Late Holocene because the hydroclimate variability in the EAM region is monsoon-dominated. If SWNA received moisture from the NAM alone we would expect there to be a similar trend in these data because of the relationship between monsoon strength and solar intensity; however, SWNA got wetter as the EAM region got drier. SWNA therefore must have been receiving moisture from an additional source and it is thus likely that the observed increase in effective moisture in SWNA during the Late Holocene came from increased winter precipitation.

It is necessary to note that the δ^{234}U signal is source (decay)-limited and could deplete over time from preferential groundwater leaching of ^{234}U regardless of any changes in the climate. However, we suggest the δ^{234}U record from stalagmite PD3 is a climate signal based on comparison with δ^{234}U data from PP1, a stalagmite collected from a cave adjacent to the cave from which stalagmite PD3 was collected. PP1 roughly follows the summer insolation curve (Fig. 14); both insolation and PP1 δ^{234}U values increase from 12 ka to 6 ka, then peak and begin decreasing from 6 ka to the present. This correlation suggests the $\delta^{234}U$ signal is responding to changes in the climate. Both $\delta^{234}U$ records from PD3 and PP1 decrease over the last 6000 years (Fig. xx).

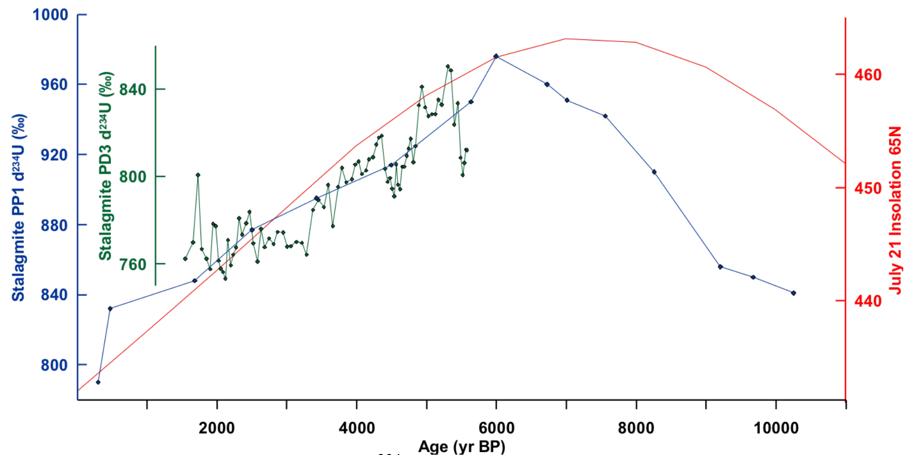

Figure 14 Stalagmites PP1 and PD3 $\delta^{234}U$ data compared to summer insolation.

In order to test the hypothesis that more winter precipitation was introduced into SWNA during the Late Holocene we used speleothem $\delta^{18}O$ data from Leviathan Cave, an alpine cave in south-central Nevada, which is interpreted as a proxy for temperature and moisture source for winter precipitation in the Great Basin (Fig. 13; Lachniet et al., 2014). Leviathan cave receives the same Pacific winter moisture as SWNA and very little addition of summer precipitation because NAM circulation does not extend that far north. The climate is therefore controlled predominantly by winter precipitation and this site provides a record of temperature and season-specific moisture that could indicate changes in the Pacific teleconnections that affect winter moisture in SWNA.

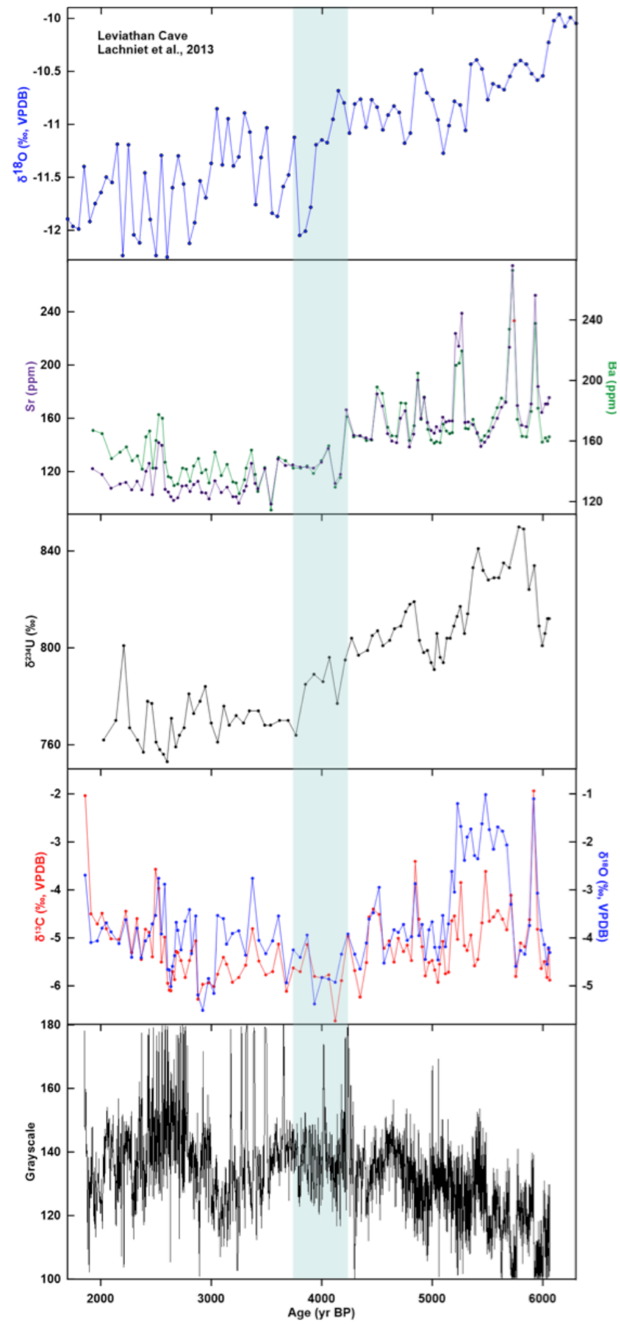

Figure 15 δ^{18}O data from Leviathan cave (top) compared to stalagmite PD3 data. The Leviathan data shows a decrease in values and increase in variability from the Middle to Late Holocene similar to the stalagmite PD3 records.

The data from Leviathan Cave shows an abrupt shift to cooler and wetter conditions between 4200 and 3800 yr BP when the $\delta^{18}O$ values decrease by ~2‰. Sampling resolution prevents the detection of interdecadal periodicities, however a clear visual increase in stalagmite growth and variability begins around 4000 yr BP (Fig. 15) that is interpreted as a result of decreasing insolation and Pacific SST changes that produced more El Nino-like conditions during the Late Holocene (Kirby et al., 2015).

This record provides evidence that the increase in effective moisture observed in the Late Holocene in stalagmites from SWNA is a result of increased winter precipitation, given that SWNA shares the same winter moisture as Leviathan cave. The high frequency, large-amplitude variability recorded in the Late Holocene is likely attributed to the proposed increase in ENSO/PDO variability (Kirby et al., 2015; Conroy et al., 2008; Clement et al., 2000), which is demonstrated to effect winter precipitation in the modern climate.

Periodic signals observed in stalagmite records in this study are consistent with known solar cycles, which suggest the climate of SWNA is sensitive to changes in solar intensity. It is also likely that summer insolation is a driver of increased Middle Holocene monsoonal precipitation input and that Pacific SSTs become increasingly important in the Late Holocene. Studies by Clement et al. (2000) and Liu et al. (2000, 2003) suggest ENSO variability was present throughout the Holocene but that ENSO variability was suppressed by solar insolation during the Middle Holocene, and then increased in strength and variability during the Late Holocene. They suggest Middle Holocene El Niño events were less frequent and less extreme, and La Niña conditions were enhanced, which is also evident in sand proxy data from a lake in the Galapagos Islands (Conroy et al., 2008). Figure 16 shows percent sand from El Junco Lake compared to stalagmites X2 and X3 stable isotope data.

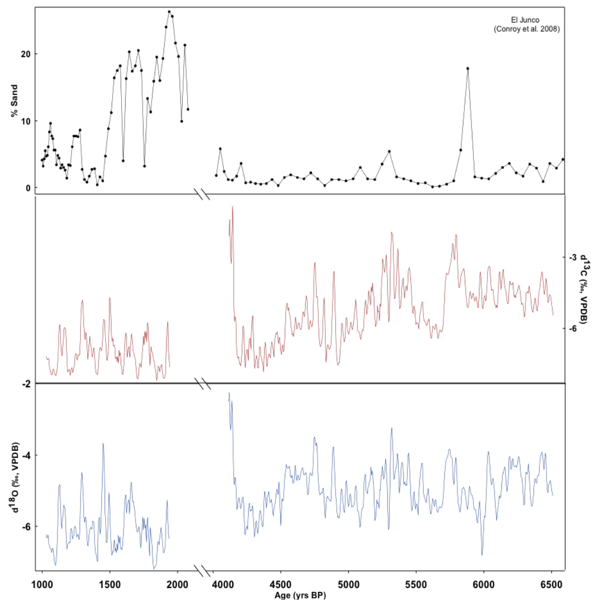

Figure 16 Sand proxy data from the Galapagos Islands (Conroy et al., 2008) displayed with X2 and X3 stable isotope data. Higher percent sand indicates higher frequency of El Nino conditions during the Late Holocene.

Higher percent sand indicates more El Niños (Conroy et al., 2008). There is a general lack of strong El Niño events during the Middle Holocene except for around ~6000 yr BP, and a clear increase in El Niño events during the Late Holocene from ~2000-1400 yr BP that corresponds with the high frequency variability observed in stalagmite X3 and BC11 records. The peaks in El Niño events observed in the sand proxy data roughly correspond with low $\delta^{18}O$ values in the Late Holocene speleothem record, which is consistent with the known expression of El Niño in SWNA. Further, SST reconstructions from the North Pacific (Barron et al., 2003) and tropical Pacific (Koutavas and Joanides, 2012) provide records of PDO and ENSO inferred activity, respectively. Warmer temperatures in the North Pacific represent positive PDO conditions along with a weaker tropical Pacific SST gradient that suggest El Niño-like conditions. The coolest North Pacific temperatures and strongest tropical Pacific SST gradient are observed in those records occurs during the warm Middle Holocene, suggesting a more negative PDO combined with La Niña-like conditions for this period. This combined PDO/ENSO effect would amplify arid conditions in SWNA, which is observed in this speleothem record. These stalagmites also record high frequency variability in the Late Holocene that is consistent with the onset of stronger ENSO/PDO activity starting around 4000 yr BP (Gliganic et al., 2014; Barron and Anderson, 2011; Conroy et al., 2008). The increase in Pacific activity driving more winter storms during the Late Holocene could explain the shift to lighter isotope values and inferred increased winter precipitation observed in stalagmite records from SWNA.

Our data also provides evidence that SWNA did experience a climate shift around 4200 yr BP that, in a global context, is consistent with various records that discuss the importance of climate change during this period with respect to the development, sustainability, and collapse of civilizations. For example, Mayewski et al. (2004) described an interval of rapid climate change at 4200-3800 yr BP that was characterized by warming in the Arctic and associated with lower sea ice volume and accordingly warmer and drier climates in the North Atlantic region (An et al., 2005). This is consistent with the timing of the collapse of the Akkadian empire as well as the collapse of numerous Neolithic cultures in China and other parts of Asia (Liu and Feng, 2012; Yang et al., 2015). It is also coeval with the timing of the earliest evidence for maize in SWNA (Merrill et al., 2009), which emphasizes the importance of small climate changes on cultural evolution and why it is necessary to understand the mechanisms behind these climate changes.

Modeling predictions of ENSO variability to increasing warming has remained inconclusive despite extensive and continuous efforts to determine if rising atmospheric temperatures will lead to more frequent El Niño or La Niña-like conditions (Dai, 2013; Sadekov et al., 2013; Collins et al., 2010; Timmermann et al., 1999). The complexity of atmosphere-ocean feedbacks that modulate ENSO behavior makes it difficult to model, but it is likely that one or more of them will be modified by anthropogenic climate change (Collins et al., 2010), demonstrating why understanding the conditions driving its behavior in the past is critical part of constraining the scope of changes in the future. A large majority of modeling experiments suggests that warming from increased greenhouse gases will result in a weakening of the Walker circulation (Sadekov et al., 2013; Collins et al., 2010; An et al., 2008; Vecchi et al., 2006), which would decrease the tropical pacific SST gradient. These model results and the relationship between zonal SST gradient and ENSO variability suggests that future warming would therefore lead to enhanced ENSO variability (Sadekov et al., 2013), which would increase the frequency of both drought and pluvial periods in SWNA. This does not necessarily inform the likelihood of more El Niño or La Niña events, which will be dependent on preferential heating of the eastern (El Niños) or western (La Niñas) tropical Pacific.

In addition to predicting changes in ENSO behavior, the question of how increasing warming will impact the NAM is equally important with respect to SWNA climate and water availability. Data from stalagmite PD3 suggests the warmer temperatures of the Middle Holocene coincided with a monsoon-dominated climate that was notably drier than the Late Holocene when temperatures were cooler. This alone would suggest heating would return SWNA to a predominantly monsoonal-dominated climate and is supported by the findings in Asmerom et al. (2013) that suggest increased warming will be accompanied by stronger (wetter) monsoons. However, whether ENSO becomes more or less important relative to its presence in the Middle Holocene could play a major role in the overall amount of effective moisture SWNA receives.

CHAPTER 6 CONCLUSIONS

This study focused on the reconstruction of the relative effective moisture in SWNA from the Middle to Late Holocene climate using U-series dating of three stalagmites from SWNA and analyses of carbon and oxygen stable isotopes, trace elements, $\delta^{234}U$, and grayscale time-series. Trace element and $\delta^{234}U$ data from stalagmite PD3 provide a long-term climate record from ~6000-2000 yr BP that suggests that there was a subtle but observable shift in the climate of SWNA around 4200 yr BP and this latter part of the Middle Holocene was slightly warmer and more arid than the Late Holocene. Grayscale data also suggests that the Late Holocene climate experienced higher frequency interdecadal and decadal climate variability. Stable isotope data from stalagmites X2 and X3 provide additional separate high-resolution records of segments of the Middle and Late Holocene that also suggest the Middle Holocene was slightly warmer/more arid and the Late Holocene was cooler/wetter and also experienced more decadal variability. The increased interdecadal and decadal variation observed in the Late Holocene from these speleothem records is consistent with the onset of a more active ENSO/PDO system and more frequent El Niños starting around 4000 yr BP.

In general it is likely that the climate of the Middle Holocene was somewhat similar to that of the Late Holocene and the transition in SWNA was subtle. The results of this study and their comparison with other climate proxies suggest the Middle Holocene climate from 6000 to 4000 yr BP was likely dominated by NAM precipitation and the transition into the Late Holocene involved the introduction of more winter precipitation as a result of increased ENSO/PDO activity and El Niño conditions. The increased strength and/or frequency of ENSO/PDO during the Late Holocene resulted in greater climate variability due to brief pluvial and drought periods that produced an overall moist period. Overall, cooler conditions (less evaporation) in the Late Holocene plus the introduction of greater winter input resulted in slightly greater effective moisture compared to the Middle Holocene.

These results emphasize the importance of understanding how large-scale climatic teleconnections, such as ENSO and PDO, as well as global monsoon systems have evolved and varied over time, and how they affected water availability in semi-arid regions such as SWNA. Detailed climate reconstructions that extend data beyond the instrumental record provide necessary information about natural climate variability that are used to make better model predictions regarding the impact of increasing warming on water resources.

APPENDIX A: EQUATIONS

Equation S1. Stalagmite PD3 U-series polynomial age equation.

$$y = -2.54\times10^{-9}x^{6} + 1.61\times10^{-6}x^{3} - 3.83\times10^{-2}x^{4} + 4.16\times10^{-2}x^{3} + 1.99x^{2} + 55.7x + 1850$$

Equation S2. Stalagmite X2 U-series polynomial 3 age equations.

$$y = -2.17\times10^{-8}x^{6} + 5.75\times10^{-6}x^{5} - 5.33\times10^{-4}x^{4} + 2.05\times10^{-2}x^{3} - 0.302x^{2} + 8.83x + 4102$$

$$y = -1.05\times10^{-5}x^{4} + 6.08\times10^{-3}x^{3} - 1.28x^{2} + 120x - 2919$$

$$y = -4.90\times10^{-12}x^{6} + 1.12\times10^{-8}x^{5} - 8.08\times10^{-6}x^{4} + 2.69\times10^{-2}x^{3} - 4.57x^{2} + 383x - 7791$$

Equation S3. Stalagmite X3 U-series polynomial 3 age equations.

$$y = 7.24\times10^{-8}x^{5} - 3.15\times10^{-5}x^{4} + 4.56\times10^{-3}x^{3} - 0.240x^{2} + 6.28x + 966$$

$$y = -1.05\times10^{-5}x^{4} + 6.08\times10^{-3}x^{3} - 1.28x^{2} + 120x - 2919$$

$$y = 3.10\times10^{-9}x^{5} - 1.98\times10^{-6}x^{4} + 2.99\times10^{-4}x^{3} + 0.035x^{2} - 7.60x + 1617$$

APPENDIX B: SUPPLEMENTARY TABLES

Table S1 Stalagmite PD3 carbon and oxygen stable isotope data.

Age YBP	$\delta^{13}C$	$\delta^{18}O$	Age YBP	$\delta^{13}C$	$\delta^{18}O$	Age YBP	$\delta^{13}C$	$\delta^{18}O$
1900	-2.03	-2.70	3608	-5.82	-3.85	4974	-5.93	-4.46
1902	-4.50	-4.10	5026	-5.07	-3.54	4991	-5.55	-4.20
1906	-4.71	-4.06	3663	-5.57	-4.36	5062	-5.75	-4.18
1912	-4.49	-3.80	3716	-4.81	-2.76	5099	-5.72	-3.71
1921	-4.81	-3.69	3768	-5.48	-4.05	5136	-4.64	-2.62
1931	-5.02	-3.87	3818	-5.77	-4.33	5173	-4.54	-3.04
1958	-5.03	-4.12	3867	-5.70	-4.06	5211	-5.03	-1.20
1992	-4.45	-3.62	3914	-5.13	-3.54	5250	-3.85	-1.67
2031	-5.31	-4.41	3959	-6.11	-4.93	5289	-5.16	-2.39
2076	-4.60	-3.80	4003	-5.63	-4.25	5329	-5.26	-1.90
2126	-5.45	-4.41	4046	-5.71	-4.41	5370	-4.95	-1.74
2180	-4.82	-4.06	4088	-5.14	-3.94	5411	-5.58	-2.29
2237	-4.88	-3.95	4128	-5.81	-5.37	5452	-5.45	-2.36
2298	-5.40	-3.71	4167	-5.83	-4.83	5494	-4.69	-1.62
2361	-3.57	-3.53	4205	-5.77	-4.86	5537	-3.62	-1.01
2426	-3.96	-2.76	4241	-6.74	-4.92	5579	-4.65	-1.75
2493	-5.51	-3.92	4277	-5.89	-4.34	5622	-4.56	-2.15
2561	-4.99	-2.88	4312	-4.96	-3.92	5665	-4.43	-1.69
2630	-5.94	-4.66	4347	-5.68	-4.34	5709	-4.61	-1.78
2664	-6.08	-4.67	4380	-6.24	-4.65	5752	-4.83	-2.07
2699	-6.11	-5.01	4413	-5.52	-4.11	5796	-4.11	-3.30
2734	-5.70	-4.59	4429	-4.56	-3.61	5839	-5.80	-4.60
2769	-5.86	-4.38	4462	-4.40	-3.48	5883	-5.10	-4.27
2804	-5.29	-3.67	4493	-4.51	-2.95	5926	-5.19	-4.33
2839	-5.31	-3.84	4525	-5.21	-4.53	5969	-4.62	-3.74
2908	-5.47	-4.26	4556	-5.07	-4.15	6012	-1.94	-1.10
2977	-5.82	-3.65	4587	-5.50	-3.83	6055	-4.82	-3.07
3046	-5.47	-3.41	4618	-5.01	-3.89	6097	-5.63	-3.84
3079	-5.27	-4.33	4649	-5.28	-3.72	6139	-5.49	-4.14
3146	-5.06	-3.54	4680	-5.16	-4.05	6180	-5.83	-4.55
3180	-6.27	-5.19	4712	-5.47	4712	6220	-5.24	-4.20
3245	-5.97	-5.51	4743	-3.41	4743	6260	-5.88	-4.31
3309	-5.94	-4.84	4775	-4.61	-3.95			
3372	-6.01	-5.15	4807	-5.18	-3.72			
3403	-5.76	-3.54	4839	-5.79	-4.45			
3463	-5.40	-3.60	4872	-5.51	-3.83			
3493	-5.54	-4.13	4906	-5.47	-3.66			
3551	-5.92	-3.90	4939	-5.67	-4.19			

Table S2 Stalagmite PD3 trace element data.

Age YBP	Sr (ppm)	Ba (ppm)	Age YBP	Sr (ppm)	Ba (ppm)
1908	122±0.19	167.1±0.61	4372	147.4±0.56	162.7±0.18
1924	117.6±0.58	165±0.63	4405	146.8±0.26	163.5±0.20
1946	107.4±0.29	148.3±0.47	4436	145.1±0.27	160.2±0.19
1978	110.7±1.30	152.7±0.80	4469	144.2±0.08	160.7±0.85
2014	112±1.31	156±0.78	4501	178.3±0.58	195.6±0.23
2058	106.1±0.31	147.1±0.62	4533	169.1±0.61	191.6±1.42
2107	112.6±0.19	150±0.11	4564	148.5±0.65	169±0.38
2158	106.3±0.30	141.5±0.90	4595	142.9±0.44	163.6±0.19
2214	120.1±0.29	162.6±0.28	4620	141.6±0.22	163.1±0.12
2275	126.1±0.19	166.6±0.33	4651	160±0.75	185.1±0.26
2341	102.6±103	142.2±0.21	4681	165.6±0.36	185±0.98
2407	122.7±0.51	160.3±0.65	4711	138.5±0.61	160.3±0.52
2471	141.6±0.43	177.5±0.93	4745	147.9±0.46	170±0.41
2540	139.7±0.28	175±0.43	4777	188.7±0.13	204.7±0.82
2540	106.6±0.05	146.1±0.45	4810	159.9±0.5	174.5±0.26
2607	104.5±0.44	136.6±0.93	4841	175.4±0.45	189±0.71
2680	100.9±0.22	136±0.25	4875	156.6±0.17	167.8±0.92
2752	98.41±0.64	130.7±0.15	4907	150.7±0.84	160.8±0.47
2820	100.1±0.25	131.7±0.44	4940	148.7±0.17	158.6±0.45
2887	108.9±0.03	142.3±1.17	4975	153.6±0.41	159.7±0.08
2958	109.5±0.46	141.5±0.92	5012	150.6±0.73	158.8±0.56
3022	105.2±0.13	133.4±0.24	5045	160.7±0.22	171.1±.047
3088	110.2±0.64	143.4±1.00	5081	157.3±0.38	166.5±0.76
3153	112.5±0.72	148.6±1.23	5118	158.2±0.42	165±0.63
3223	104.2±0.07	139.1±1.18	5156	158.2±0.22	165.5±0.54
3285	103.7±0.59	140.9±1.09	5197	223.6±0.13	210.2±0.74
3347	99.39±0.26	132.3±1.20	5235	214.3±1.07	211.3±0.43
3410	112.9±0.46	152.5±0.32	5275	238.8±1.34	219.5±0.21
3471	104.1±0.16	137.3±0.82	5314	156.6±0.56	168.4±0.05
3531	108.4±0.53	144.6±0.18	5353	157.3±0.46	167.9±0.55
3587	101±0.33	132.9±0.24	5412	155.3±0.36	174.2±0.43
3610	101.1±0.24	132.2±0.78	5452	149.3±0.68	165±0.51
3643	96.47±0.29	125.3±0.35	5493	138.7±0.51	160.3±0.28
3698	105.4±0.15	134.3±0.33	5536	142.1±0.25	163.5±0.57
3707	108.9±0.28	142.2±0.72	5581	145.9±0.54	166.7±0.98
3747	126.1±0.53	153.9±0.22	5623	153.4±1.45	175.3±0.64
3770	111.1±0.21	138.1±0.49	5669	160±0.09	182.1±0.45
3799	107±0.42	126.6±0.05	5709	168.3±0.45	188.5±0.80
3851	122.2±0.54	142.6±0.25	5757	171.9±0.12	185.9±0.54
3899	95.29±0.24	114.6±0.25	5800	213.5±0.43	234±1.00

3946	129.3±0.11	149.2±0.66	5831	274.6±1.6	272.7±1.44
3990	124.7±0.27	147±0.49	5874	169.6±0.84	174.4±0.38
4032	124.8±0.35	142.2±0.33	5916	154.7±0.39	163.3±0.68
4073	123.5±0.25	142.1±0.85	5958	153.8±0.26	162.9±0.48
4117	123.3±0.72	143.6±0.39	6002	170.8±0.7	179.6±1.57
4156	122.5±0.07	138.5±0.20	6045	252.3±0.35	237.6±0.40
4193	126.9±0.17	146.9±0.87	6081	183.8±1	181.8±0.96
4232	137.4±0.32	156.8±0.84	6123	164.5±0.29	159.4±0.35
4268	111.2±0.64	129.4±1.18	6165	170.8±0.2	161.9±0.67
4303	118±0.21	136±0.10	6204	170.8±0.28	159.9±0.55
4338	166.2±0.48	176.2±1.01	6245	175.6±0.38	162.8±0.87

Table S3 Stalagmite PD3 $\delta^{234}U$ data

Age YBP	δ234U ‰	Age YBP	δ234U ‰	Age YBP	δ234U ‰
1916	762±1.76	3821	768±2.74	4952	806±2.76
1949	770±2.43	3865	768±2.26	4990	796±5.31
1983	801±2.60	3918	770±3.54	5028	794±2.64
2024	767±3.06	3974	770±0.14	5068	804±2.67
2093	762±1.69	4022	764±3.73	5108	804±2.33
2161	757±2.37	4080	785±2.86	5152	809±1.61
2225	778±2.78	4131	789±1.78	5192	813±1.63
2307	777±1.87	4174	786±0.15	5233	817±1.07
2385	761±2.90	4213	796±2.70	5276	806±3.09
2463	758±2.27	4258	777±1.88	5326	814±1.46
2546	756±3.23	4296	795±1.51	5391	833±3.25
2633	753±0.54	4335	804±3.00	5445	841±4.14
2713	771±3.94	4374	797±1.06	5498	832±1.46
2810	759±2.34	4424	799±2.48	5552	828±3.66
2893	764±2.81	4453	805±3.68	5614	829±5.53
2960	767±3.31	4484	807±5.08	5661	829±5.53
3044	781±2.93	4516	801±2.10	5709	829±4.85
3123	773±2.13	4554	803±2.63	5757	833±3.96
3210	778±1.89	4588	808±3.64	5808	935±15.4
3281	784±0.13	4628	809±2.18	5852	850±3.28
3351	769±1.77	4663	815±1.58	5906	849±2.11
3416	761±2.85	4696	818±1.07	5953	824±10.6
3472	776±2.88	4730	819±2.08	6006	834±1.65
3531	768±1.30	4776	803±2.08	6053	809±4.66
3587	772±3.55	4813	798±1.68	6101	801±4.30
3650	769±2.42	4851	799±2.71	6136	806±2.77
3705	774±2.10	4883	794±2.64	6183	812±2.98
3769	774±0.15	4920	791±2.38	6217	812±2.98

Table S4 Stalagmite X2 carbon and oxygen stable isotope data.

Age YBP	$\delta^{13}C$	$\delta^{18}O$	Age YBP	$\delta^{13}C$	$\delta^{18}O$	Age YBP	$\delta^{13}C$	$\delta^{18}O$	Age YBP	$\delta^{13}C$	$\delta^{18}O$
4106	-4.50	-3.34	4262	-7.44	-6.02	4428	-8.12	-5.73	4528	-5.17	-3.79
4111	-2.99	-3.01	4266	-4.43	-4.72	4431	-4.91	-4.95	4531	-6.46	-5.01
4115	-1.55	-2.38	4270	-6.96	-5.34	4434	-6.20	-5.15	4533	-5.47	-4.69
4119	-3.09	-2.52	4275	-7.20	-5.67	4437	-6.52	-5.05	4536	-5.10	-4.19
4122	1.70	-1.15	4279	-7.58	-6.11	4440	-7.57	-5.81	4539	-5.04	-4.64
4126	-2.16	-2.70	4283	-3.12	-4.65	4443	-7.06	-5.56	4542	-2.77	-3.90
4130	-6.23	-4.90	4288	-6.17	-6.00	4446	-7.07	-5.77	4544	-5.23	-3.79
4134	-3.57	-3.02	4292	-5.65	-5.43	4449	-7.17	-5.61	4547	-5.65	-4.57
4137	-0.11	-2.01	4297	-6.48	-5.25	4452	-6.73	-5.61	4550	-5.15	-4.62
4141	3.28	-0.67	4301	-7.77	-6.34	4454	-5.50	-5.39	4554	-4.95	-4.35
4144	-1.35	-3.35	4305	-8.20	-6.65	4457	-5.42	-4.75	4557	-5.79	-4.65
4148	-6.23	-4.99	4310	-7.43	-6.19	4460	-6.68	-5.47	4560	-4.97	-4.06
4151	-5.98	-4.39	4314	-6.51	-5.77	4462	-7.01	-5.54	4563	-5.73	-4.33
4155	-6.89	-5.29	4318	-7.05	-5.55	4465	-6.54	-5.38	4567	-6.07	-4.67
4158	-5.37	-4.62	4323	-7.84	-6.07	4467	-5.43	-4.67	4571	-5.54	-4.30
4162	-3.03	-4.63	4327	-7.72	-6.07	4470	-5.49	-4.35	4574	-6.40	-5.17
4165	-5.42	-3.97	4331	-7.91	-6.37	4472	-5.84	-5.27	4578	-5.74	-4.20
4169	-7.07	-5.37	4336	-7.28	-6.23	4475	-6.43	-5.13	4582	-6.66	-4.72
4172	-7.52	-5.66	4340	-6.45	-5.73	4477	-6.86	-5.39	4586	-6.31	-4.49
4176	-7.68	-5.64	4344	-6.26	-5.03	4479	-7.73	-5.97	4590	-6.08	-4.70
4179	-6.38	-5.34	4349	-7.41	-5.68	4481	-6.73	-5.01	4595	-6.60	-5.13
4183	-7.57	-5.83	4353	-7.87	-6.03	4484	-6.83	-5.04	4599	-5.88	-4.53
4187	-7.35	-4.75	4357	-7.27	-5.63	4486	-5.73	-4.41	4604	-5.36	-4.43
4190	-7.45	-4.93	4361	-6.49	-5.71	4488	-5.86	-4.34	4609	-5.31	-3.83
4194	-7.68	-5.44	4365	-8.04	-6.31	4490	-5.67	-4.05	4613	-5.90	-4.64
4198	-7.40	-5.27	4369	-8.20	-6.27	4493	-6.35	-5.16	4618	-6.80	-5.39
4201	-7.44	-5.36	4373	-7.47	-5.43	4495	-7.22	-6.07	4624	-5.47	-4.19
4205	-7.74	-5.65	4377	-7.46	-5.54	4497	-7.60	-6.20	4629	-5.43	-4.34
4209	-7.05	-5.69	4381	-4.51	-4.33	4499	-7.80	-6.57	4634	-6.31	-5.14
4213	-6.15	-5.11	4385	-7.04	-4.96	4501	-7.80	-6.47	4640	-5.84	-4.55
4217	-6.43	-5.14	4389	-8.06	-5.62	4503	-6.94	-5.31	4646	-6.13	-4.49
4221	-4.25	-4.81	4393	-7.25	-5.62	4505	-6.32	-5.34	4651	-6.26	-4.78
4225	-6.61	-5.50	4396	-7.51	-5.11	4508	-5.28	-4.42	4657	-5.12	-3.92
4229	-7.08	-5.56	4400	-7.57	-5.55	4510	-6.41	-4.77	4664	-5.21	-4.65
4233	-7.72	-6.29	4404	-6.89	-4.83	4512	-6.13	-4.26	4670	-5.57	-4.45
4237	-8.38	-6.70	4407	-6.87	-4.72	4514	-6.95	-5.22	4676	-5.73	-4.66
4241	-7.46	-6.40	4411	-7.19	-5.02	4516	-7.75	-5.89	4683	-4.34	-4.42
4245	-5.74	-5.44	4414	-7.12	-5.23	4519	-7.32	-5.70	4689	-4.37	-4.43
4249	-7.06	-5.98	4418	-7.76	-5.57	4521	-7.18	-5.40	4696	-5.77	-4.99
4253	-8.11	-6.91	4421	-6.72	-5.19	4523	-6.53	-4.91	4701	-6.44	-5.43

4258	-6.86	-5.47	4424	-7.18	-5.29	4526	-5.94	-4.52	4709	-5.79	-4.79
4717	-5.39	-4.28	4986	-5.98	-4.82	5111	-5.38	-4.80	5211	-4.98	-5.03
4724	-6.30	-4.65	4990	-6.18	-5.20	5113	-5.15	-4.59	5214	-3.74	-5.01
4732	-5.69	-4.59	4995	-6.21	-5.20	5116	-5.67	-5.08	5217	-4.79	-4.82
4740	-5.43	-4.36	4999	-6.12	-5.50	5118	-5.50	-4.78	5219	-6.25	-5.79
4748	-0.72	-2.62	5003	-6.42	-5.63	5120	-4.28	-4.00	5222	-6.42	-5.74
4756	-5.84	-4.37	5007	-6.27	-5.60	5123	-5.28	-4.66	5225	-5.38	-5.29
4764	-3.82	-3.19	5011	-5.38	-4.76	5125	-5.23	-4.94	5228	-4.43	-4.86
4772	-5.55	-4.11	5015	-5.48	-4.80	5127	-4.84	-4.55	5231	-5.85	-5.71
4779	-6.55	-5.07	5019	-6.02	-5.46	5130	-4.92	-4.66	5234	-3.93	-3.97
4787	-6.79	-5.12	5022	-6.44	-5.61	5132	-6.31	-5.66	5237	-4.68	-4.65
4795	-6.80	-5.12	5026	-6.20	-5.49	5135	-6.10	-5.44	5240	-5.71	-5.33
4803	-6.31	-4.97	5029	-5.82	-5.42	5137	-5.93	-5.47	5243	-6.30	-5.76
4810	-6.32	-5.15	5033	-5.65	-5.28	5139	-4.95	-4.81	5246	-1.35	-3.46
4818	-2.39	-4.44	5036	-5.76	-5.46	5142	-4.14	-5.30	5249	-2.74	-4.08
4825	-7.92	-6.16	5040	-5.83	-5.53	5144	-4.46	-5.19	5253	-3.29	-4.43
4832	-7.24	-5.64	5043	-5.77	-5.77	5147	-3.25	-4.17	5256	-3.34	-4.59
4839	-6.55	-4.99	5046	-3.94	-5.02	5149	-4.26	-4.95	5259	-3.84	-4.77
4847	-6.73	-5.27	5049	-5.12	-5.03	5152	-4.94	-4.82	5262	-3.79	-4.69
4854	-6.92	-5.19	5052	-5.49	-4.96	5154	-5.30	-4.85	5266	-3.80	-4.77
4861	-6.93	-5.32	5055	-4.57	-4.37	5156	-5.51	-4.92	5269	-2.94	-4.29
4867	-6.66	-5.27	5058	-4.97	-4.41	5159	-4.33	-4.38	5273	-3.21	-4.46
4874	-6.71	-5.42	5061	-6.07	-5.65	5161	-4.71	-4.60	5276	-2.99	-3.98
4881	-3.84	-3.75	5064	-5.97	-5.46	5163	-5.35	-4.57	5280	-2.57	-3.87
4887	-3.26	-3.60	5067	-5.98	-5.50	5166	-5.09	-4.77	5283	-4.15	-4.80
4894	-3.49	-3.83	5069	-6.62	-5.97	5168	-2.68	-3.24	5287	-4.80	-5.15
4900	-6.30	-4.74	5072	-6.49	-5.87	5170	-3.07	-3.80	5290	-5.56	-5.86
4906	-6.74	-5.02	5075	-5.89	-5.32	5173	-3.60	-4.09	5294	-5.79	-6.06
4912	-7.73	-5.67	5077	-6.12	-5.68	5175	-5.19	-5.20	5298	-6.11	-6.39
4918	-7.44	-5.64	5080	-6.04	-5.54	5178	-4.09	-4.34	5301	-5.61	-6.24
4924	-7.68	-5.91	5082	-7.30	-6.42	5180	-3.99	-4.36	5305	-4.64	-5.63
4930	-7.24	-5.61	5085	-6.89	-6.40	5182	-4.39	-4.51	5309	-0.16	-3.03
4936	-7.54	-5.92	5087	-6.76	-6.24	5185	-4.34	-4.37	5313	-3.54	-4.04
4941	-6.13	-5.49	5090	-6.49	-6.15	5187	-4.52	-4.80	5316	-2.50	-2.85
4946	-5.15	-4.56	5092	-6.26	-5.81	5190	-5.73	-5.65	5320	-1.98	-3.61
4952	-5.89	-4.86	5095	-5.83	-5.33	5192	-5.09	-5.26	5324	-0.72	-2.64
4957	-6.80	-5.66	5097	-5.48	-4.90	5195	-5.88	-5.79	5328	-2.76	-3.41
4962	-5.96	-4.94	5099	-6.34	-5.66	5198	-6.29	-6.09	5332	-5.13	-4.99
4967	-6.63	-5.73	5102	-5.68	-5.07	5200	-6.19	-6.08	5336	-5.06	-4.88
4972	-7.34	-6.28	5104	-6.19	-5.71	5203	-5.25	-5.37	5340	-5.23	-4.93
4977	-5.16	-4.74	5106	-6.36	-5.69	5206	-5.67	-5.51	5344	-3.69	-4.10
4981	-4.79	-4.14	5109	-6.51	-5.83	5208	-6.61	-6.01	5349	-4.26	-4.34
5353	-4.33	-4.50	5552	-6.11	-5.34	5785	-2.70	-4.54	6019	-3.75	-4.67

5357	-4.33	-4.54	5557	-5.50	-5.20	5791	-1.20	-3.65	6025	-3.46	-4.37
5361	-0.85	-3.88	5563	-5.64	-4.99	5796	-2.19	-3.94	6030	-3.58	-3.90
5366	-2.11	-3.15	5568	-5.97	-5.46	5802	-3.23	-4.98	6036	-3.20	-3.70
5370	-4.76	-4.80	5574	-5.78	-5.27	5808	-3.93	-5.32	6041	-3.32	-4.14
5374	-5.23	-4.96	5579	-6.06	-5.43	5814	-4.58	-5.49	6047	-3.76	-4.34
5379	-5.76	-5.61	5585	-5.34	-4.78	5820	-4.24	-5.45	6052	-4.92	-5.12
5383	-4.50	-4.43	5590	-5.83	-5.08	5826	-3.62	-5.82	6058	-4.21	-4.68
5388	-4.43	-4.33	5596	-5.58	-4.91	5831	-3.58	-5.53	6063	-4.22	-5.00
5392	-4.58	-4.63	5601	-6.26	-5.57	5837	-3.81	-4.91	6068	-4.36	-4.31
5397	-3.41	-3.88	5607	-6.78	-5.89	5843	-3.48	-4.81	6074	-4.99	-4.72
5401	-3.69	-4.04	5612	-6.29	-5.56	5849	-3.36	-5.11	6079	-5.44	-5.36
5406	-4.27	-4.54	5618	-6.06	-5.39	5855	-3.61	-4.75	6085	-4.66	-5.05
5410	-5.07	-4.81	5624	-5.50	-4.86	5860	-4.33	-5.06	6090	-5.43	-5.98
5415	-4.98	-5.23	5629	-6.29	-5.55	5866	-4.69	-5.31	6095	-4.99	-5.61
5420	-3.43	-4.20	5635	-6.10	-5.53	5872	-4.88	-5.23	6101	-4.99	-5.99
5424	-4.18	-5.05	5641	-5.73	-5.22	5878	-5.42	-5.72	6106	-3.91	-5.30
5429	-5.06	-5.35	5646	-5.58	-5.07	5883	-5.08	-5.63	6111	-3.41	-5.09
5434	-4.12	-4.36	5652	-6.43	-5.57	5889	-4.68	-4.97	6117	-3.42	-5.28
5439	-3.58	-4.16	5658	-6.57	-5.68	5895	-4.16	-4.70	6122	-4.26	-4.93
5444	-3.12	-3.63	5663	-6.45	-5.64	5901	-4.67	-5.06	6127	-5.58	-5.63
5449	-3.54	-3.93	5669	-5.90	-5.37	5906	-5.08	-5.26	6133	-2.62	-4.45
5453	-3.94	-4.57	5675	-6.08	-5.45	5912	-4.44	-4.96	6138	-3.44	-4.54
5458	-4.15	-5.03	5681	-6.20	-5.54	5918	-4.40	-5.19	6143	-3.83	-4.48
5463	-4.11	-4.89	5686	-6.11	-5.43	5924	-4.66	-5.38	6149	-4.40	-4.62
5468	-5.81	-6.07	5692	-6.22	-5.48	5929	-5.15	-5.68	6154	-4.22	-4.14
5473	-5.68	-5.70	5698	-5.84	-5.38	5935	-4.73	-5.50	6159	-4.42	-4.23
5478	-5.04	-4.96	5704	-4.57	-4.93	5941	-4.39	-5.40	6164	-4.60	-4.65
5484	-4.73	-4.74	5709	-4.56	-4.73	5946	-4.91	-5.77	6169	-4.97	-5.20
5489	-5.36	-5.28	5715	-3.50	-4.24	5952	-5.34	-6.04	6175	-5.13	-5.15
5494	-6.00	-5.74	5721	-3.86	-4.17	5958	-5.37	-5.98	6180	-4.77	-4.31
5499	-6.22	-5.65	5727	-3.66	-4.23	5963	-4.10	-5.43	6185	-4.66	-4.61
5504	-5.18	-4.86	5732	-3.59	-3.76	5969	-3.31	-5.14	6190	-3.16	-3.38
5509	-5.87	-5.59	5738	-4.02	-4.24	5975	-3.65	-5.37	6196	-4.40	-4.25
5515	-6.29	-5.81	5744	-3.17	-3.54	5980	-4.59	-6.27	6201	-5.31	-5.06
5520	-5.87	-5.60	5750	-3.33	-3.88	5986	-5.26	-7.14	6206	-2.57	-3.99
5525	-4.87	-4.19	5756	-3.31	-4.16	5991	-5.73	-7.22	6211	-4.63	-4.05
5530	-5.28	-4.63	5762	-2.71	-4.07	5997	-4.21	-5.36	6216	-4.95	-4.22
5536	-5.74	-5.04	5767	-1.71	-3.85	6003	-4.92	-6.10	6221	-3.83	-4.05
5541	-3.80	-3.39	5773	-2.79	-4.65	6008	-4.21	-5.35	6227	-5.71	-4.85
5546	-5.06	-4.17	5779	-3.73	-5.21	6014	-5.61	-6.13	6232	-3.98	-3.87
6237	-4.68	-4.34	6304	-5.08	-5.06	6372	-4.80	-4.90	6444	-4.88	-4.59
6242	-4.51	-4.54	6309	-4.22	-3.90	6378	-4.51	-4.43	6450	-4.23	-4.23
6247	-4.64	-4.35	6314	-4.26	-4.52	6383	-4.88	-4.64	6456	-3.46	-3.48

6252	-3.95	-3.86	6320	-4.97	-4.91	6389	-5.79	-5.14	6462	-4.04	-4.25
6258	-4.26	-4.23	6325	-3.98	-4.12	6394	-5.11	-4.58	6468	-5.49	-5.43
6263	-4.14	-3.79	6330	-4.60	-4.36	6400	-4.43	-4.27	6474	-4.76	-4.87
6268	-4.84	-4.39	6335	-4.07	-4.25	6405	-4.47	-4.94	6480	-4.66	-5.04
6273	-4.97	-4.57	6341	-4.82	-5.22	6411	-4.27	-4.47	6486	-4.34	-4.49
6278	-5.26	-4.87	6346	-4.89	-5.26	6416	-3.99	-3.92	6492	-4.89	-4.84
6283	-4.63	-4.36	6351	-5.16	-5.28	6422	-3.65	-4.03	6498	-4.80	-4.84
6288	-4.88	-4.69	6356	-5.45	-5.59	6427	-3.54	-4.06	6504	-5.32	-5.11
6294	-5.71	-5.59	6362	-5.41	-5.47	6433	-3.48	-3.60	6510	-5.48	-5.16
6299	-5.84	-5.74	6367	-4.94	-4.85	6439	-4.68	-4.44	6516	-5.59	-5.17

Table S5 Stalagmite X3 carbon and oxygen stable isotope data.

Age YBP	$\delta^{13}C$	$\delta^{18}O$	Age YBP	$\delta^{13}C$	$\delta^{18}O$	Age YBP	$\delta^{13}C$	$\delta^{18}O$	Age YBP	$\delta^{13}C$	$\delta^{18}O$
1024	-6.49	-5.68	1154	-5.83	-4.94	1288	-4.01	-4.29	1425	-5.90	-5.58
1028	-7.08	-6.19	1157	-6.13	-5.68	1292	-5.07	-4.85	1429	-7.15	-6.84
1032	-7.59	-6.51	1160	-6.25	-5.71	1295	-5.16	-4.63	1432	-7.26	-6.82
1035	-7.96	-6.86	1164	-6.12	-5.57	1299	-4.99	-4.31	1436	-6.31	-4.52
1039	-6.92	-5.95	1167	-5.45	-5.16	1302	-4.82	-4.51	1439	-6.94	-5.63
1042	-7.16	-6.17	1170	-5.77	-5.19	1306	-6.60	-5.86	1442	-6.70	-5.37
1046	-7.19	-6.28	1174	-6.39	-5.70	1309	-7.05	-6.10	1446	-6.63	-4.75
1049	-7.67	-6.51	1177	-7.39	-6.55	1313	-6.76	-6.15	1449	-5.47	-2.82
1052	-7.99	-6.79	1180	-7.52	-6.60	1316	-5.39	-5.20	1453	-3.60	-2.52
1056	-7.97	-6.72	1184	-7.93	-6.72	1320	-6.43	-5.96	1456	-6.16	-3.50
1059	-7.60	-6.32	1187	-8.08	-6.71	1324	-5.84	-5.50	1459	-6.80	-5.70
1062	-8.15	-6.82	1190	-8.14	-6.53	1327	-7.51	-6.61	1463	-7.06	-5.98
1066	-7.97	-6.64	1194	-7.20	-6.11	1331	-6.28	-5.70	1466	-3.53	-3.76
1069	-8.14	-6.85	1197	-7.84	-6.69	1334	-7.84	-7.04	1469	-7.36	-6.53
1072	-7.83	-6.79	1201	-8.07	-6.67	1338	-7.64	-6.67	1473	-7.61	-6.50
1076	-7.63	-6.43	1204	-8.04	-6.51	1341	-6.77	-6.25	1476	-7.08	-6.35
1079	-7.49	-6.42	1207	-8.17	-6.37	1345	-5.76	-6.15	1479	-7.57	-6.67
1082	-7.93	-6.93	1211	-7.72	-6.04	1349	-6.87	-6.34	1483	-7.01	-6.17
1086	-7.91	-6.73	1214	-7.31	-5.78	1352	-5.65	-5.84	1486	-7.32	-6.41
1089	-7.91	-6.99	1218	-7.79	-6.21	1356	-6.73	-6.00	1489	-6.13	-5.55
1092	-7.91	-7.05	1221	-7.63	-6.07	1359	-7.03	-6.03	1492	-5.89	-5.65
1095	-7.97	-7.01	1225	-7.98	-6.44	1363	-7.16	-6.06	1496	-4.71	-4.67
1098	-8.06	-7.08	1228	-7.95	-6.52	1366	-7.55	-6.22	1499	-2.55	-4.39
1102	-8.06	-7.13	1232	-8.00	-6.61	1370	-7.23	-6.06	1502	-5.36	-5.69
1105	-7.95	-7.17	1235	-6.70	-5.59	1373	-6.89	-5.92	1505	-7.19	-7.01
1108	-7.52	-6.77	1239	-7.47	-6.32	1377	-7.37	-6.21	1509	-7.27	-7.18
1111	-7.27	-6.27	1242	-8.27	-6.62	1380	-5.91	-5.06	1512	-7.76	-7.76
1115	-7.08	-6.17	1246	-5.60	-5.11	1384	-7.00	-6.13	1515	-4.02	-5.18
1118	-7.25	-6.06	1249	-6.83	-5.87	1387	-7.97	-6.79	1518	-7.12	-7.15
1121	-6.48	-5.42	1253	-8.02	-6.80	1391	-7.88	-6.91	1521	-6.87	-7.08
1124	-4.48	-3.88	1256	-7.25	-6.22	1394	-7.96	-6.71	1525	-6.92	-6.95
1128	-6.28	-5.09	1260	-7.58	-6.53	1398	-7.89	-6.66	1528	-6.17	-5.97
1131	-5.39	-4.31	1263	-6.53	-5.78	1401	-7.58	-6.70	1531	-6.41	-6.17
1134	-7.03	-5.71	1267	-6.30	-5.70	1405	-8.08	-7.06	1534	-7.02	-6.57
1137	-6.78	-5.72	1270	-7.82	-6.82	1408	-8.05	-7.13	1537	-6.67	-6.11
1141	-7.13	-5.86	1274	-7.81	-6.86	1412	-8.37	-7.32	1541	-7.75	-6.99
1144	-7.08	-5.95	1277	-5.79	-5.68	1415	-7.16	-6.56	1544	-7.91	-7.15
1147	-7.70	-6.49	1281	-7.01	-6.12	1419	-6.36	-3.97	1547	-5.02	-5.23
1150	-7.31	-6.38	1284	-5.27	-4.86	1422	-7.83	-6.88	1550	-7.62	-6.86
1553	-7.77	-6.90	1677	-6.58	-4.91	1811	-6.73	-6.31	1664	-7.13	-5.52

1556	-7.93	-6.94	1680	-7.49	-5.69	1814	-7.87	-7.20	1667	-7.74	-5.87
1560	-6.87	-6.12	1683	-6.67	-4.97	1818	-6.18	-6.00	1670	-5.79	-4.28
1563	-7.60	-6.99	1686	-7.62	-5.97	1821	-7.29	-7.10	1673	-7.69	-5.76
1566	-7.47	-6.67	1690	-7.74	-5.85	1825	-8.06	-7.85	1796	-7.10	-6.48
1569	-6.17	-5.63	1693	-8.04	-6.24	1829	-7.92	-7.70	1800	-7.88	-6.92
1572	-7.57	-6.83	1696	-8.44	-6.17	1832	-7.48	-7.01	1804	-6.14	-5.53
1575	-7.83	-7.02	1700	-7.74	-5.93	1836	-6.69	-6.57	1807	-7.23	-6.44
1578	-7.07	-6.23	1703	-8.35	-6.17	1839	-8.61	-7.53	1926	-7.18	-6.19
1582	-7.78	-6.68	1706	-8.38	-6.28	1843	-8.73	-7.35	1929	-6.59	-5.69
1585	-7.62	-6.63	1710	-8.14	-6.33	1846	-7.68	-6.49	1931	-7.81	-6.51
1588	-8.11	-6.89	1713	-7.53	-5.73	1850	-7.83	-6.63	1934	-7.92	-6.37
1591	-8.19	-6.92	1716	-7.34	-5.74	1853	-7.59	-6.52	1936	-8.40	-6.63
1594	-7.97	-6.42	1720	-7.14	-6.05	1857	-8.02	-6.76	1938	-7.54	-6.48
1597	-8.18	-6.60	1723	-7.77	-6.58	1860	-6.85	-5.75	1940	-7.10	-6.41
1600	-7.49	-6.04	1726	-7.89	-6.68	1864	-7.99	-6.59	1943	-6.46	-5.72
1603	-7.36	-6.03	1730	-7.59	-6.59	1867	-8.12	-6.84	1945	-7.91	-6.34
1607	-7.38	-5.97	1733	-7.64	-6.70	1871	-8.33	-6.81	1946	-7.25	-6.30
1610	-6.43	-5.52	1737	-6.94	-6.28	1874	-6.68	-5.46			
1613	-3.84	-3.96	1740	-5.60	-5.13	1877	-7.37	-5.94			
1616	-7.01	-5.47	1744	-7.05	-6.04	1881	-8.31	-6.65			
1619	-6.93	-5.30	1747	-6.17	-5.69	1884	-8.05	-6.32			
1622	-6.54	-5.17	1751	-5.79	-5.66	1887	-7.67	-6.26			
1625	-7.46	-5.79	1754	-7.22	-6.64	1891	-7.52	-6.36			
1629	-7.72	-6.05	1758	-5.10	-4.88	1894	-8.31	-6.94			
1632	-7.78	-6.12	1761	-5.41	-5.28	1897	-8.18	-6.74			
1635	-5.46	-4.08	1765	-7.17	-6.76	1900	-8.54	-7.08			
1638	-6.77	-5.23	1768	-6.54	-6.39	1903	-8.08	-6.66			
1641	-6.61	-5.23	1772	-5.54	-5.96	1906	-6.16	-5.34			
1644	-7.59	-6.00	1775	-7.04	-6.79	1909	-8.31	-6.89			
1648	-7.74	-5.96	1779	-4.55	-5.03	1912	-8.04	-6.46			
1651	-7.18	-5.68	1782	-5.35	-4.94	1915	-8.05	-6.64			
1654	-5.39	-4.02	1786	-6.89	-6.45	1918	-7.55	-6.35			
1657	-6.32	-4.76	1789	-8.79	-8.18	1921	1.64	-1.73			
1660	-5.92	-4.63	1793	-6.10	-5.34	1923	-5.94	-5.12			

Table S6 Stalagmite X2 grayscale data.

Age YBP	Grayscale	Age YBP	Grayscale	Age YBP	Grayscale	Age YBP	Grayscale
4110	144	4305	149	4500	161	4695	151
4115	59	4310	176	4505	145	4700	170
4120	129	4315	189	4510	185	4705	175
4125	102	4320	138	4515	157	4710	165
4130	84	4325	147	4520	137	4715	143
4135	129	4330	144	4525	145	4720	154
4140	58	4335	164	4530	154	4725	157
4145	87	4340	196	4535	143	4730	142
4150	159	4345	177	4540	162	4735	154
4155	160	4350	162	4545	152	4740	148
4160	153	4355	176	4550	130	4745	158
4165	112	4360	216	4555	114	4750	155
4170	163	4365	158	4560	143	4755	162
4175	166	4370	168	4565	149	4760	142
4180	156	4375	172	4570	140	4765	58
4185	160	4380	99	4575	141	4770	89
4190	150	4385	162	4580	150	4775	146
4195	149	4390	138	4585	130	4780	127
4200	152	4395	134	4590	129	4785	149
4205	154	4400	157	4595	135	4790	144
4210	154	4405	155	4600	123	4795	145
4215	160	4410	146	4605	126	4800	148
4220	161	4415	137	4610	137	4805	166
4225	165	4420	147	4615	130	4810	144
4230	110	4425	165	4620	138	4815	138
4235	145	4430	147	4625	124	4820	142
4240	167	4435	181	4630	113	4825	161
4245	174	4440	143	4635	123	4830	40
4250	184	4445	149	4640	128	4835	119
4255	191	4450	138	4645	137	4840	83
4260	178	4455	143	4650	132	4845	110
4265	172	4460	191	4655	123	4850	72
4270	184	4465	147	4660	124	4855	102
4275	197	4470	151	4665	132	4860	133
4280	192	4475	155	4670	131	4865	130
4285	158	4480	164	4675	145	4870	149
4290	180	4485	141	4680	151	4875	127
4295	173	4490	150	4685	154	4880	142
4300	130	4495	157	4690	153	4885	148
4890	142	5095	139	5300	139	5505	158

4895	149	5100	122	5305	135	5510	154
4900	134	5105	152	5310	123	5515	140
4905	87	5110	150	5315	122	5520	128
4910	146	5115	128	5320	94	5525	130
4915	74	5120	136	5325	128	5530	131
4920	154	5125	139	5330	145	5535	140
4925	142	5130	142	5335	130	5540	154
4930	148	5135	150	5340	140	5545	142
4935	140	5140	153	5345	140	5550	153
4940	143	5145	141	5350	159	5555	152
4945	146	5150	147	5355	151	5560	135
4950	132	5155	196	5360	172	5565	141
4955	148	5160	168	5365	168	5570	149
4960	141	5165	185	5370	168	5575	167
4965	150	5170	154	5375	148	5580	151
4970	137	5175	141	5380	142	5585	162
4975	137	5180	160	5385	146	5590	154
4980	141	5185	145	5390	137	5595	152
4985	140	5190	145	5395	142	5600	144
4990	121	5195	149	5400	168	5605	148
4995	149	5200	171	5405	161	5610	145
5000	146	5205	178	5410	149	5615	154
5005	162	5210	179	5415	149	5620	138
5010	149	5215	178	5420	149	5625	148
5015	163	5220	163	5425	159	5630	136
5020	159	5225	168	5430	155	5635	144
5025	153	5230	160	5435	163	5640	146
5030	142	5235	160	5440	162	5645	146
5035	144	5240	170	5445	130	5650	145
5040	136	5245	164	5450	160	5655	153
5045	149	5250	166	5455	150	5660	139
5050	142	5255	154	5460	167	5665	151
5055	142	5260	140	5465	145	5670	125
5060	176	5265	143	5470	143	5675	143
5065	140	5270	149	5475	139	5680	159
5070	136	5275	142	5480	153	5685	156
5075	130	5280	135	5485	158	5690	146
5080	133	5285	123	5490	156	5695	161
5085	141	5290	118	5495	143	5700	154
5090	145	5295	136	5500	155	5705	142
5710	178	5915	97	6120	149	6325	173
5715	143	5920	121	6125	165	6330	168
5720	152	5925	157	6130	152	6335	149

5725	144	5930	155	6135	133	6340	148
5730	168	5935	124	6140	138	6345	168
5735	147	5940	114	6145	121	6350	153
5740	118	5945	138	6150	155	6355	168
5745	174	5950	145	6155	143	6360	162
5750	165	5955	129	6160	147	6365	171
5755	88	5960	132	6165	162	6370	162
5760	54	5965	150	6170	128	6375	177
5765	163	5970	155	6175	174	6380	161
5770	151	5975	145	6180	166	6385	169
5775	150	5980	136	6185	156	6390	178
5780	143	5985	140	6190	173	6395	179
5785	87	5990	126	6195	162	6400	186
5790	125	5995	138	6200	160	6405	156
5795	53	6000	154	6205	161	6410	164
5800	85	6005	149	6210	155	6415	169
5805	86	6010	141	6215	174	6420	156
5810	85	6015	141	6220	154	6425	163
5815	88	6020	131	6225	137	6430	173
5820	91	6025	126	6230	171	6435	181
5825	98	6030	148	6235	176	6440	170
5830	121	6035	162	6240	185	6445	166
5835	141	6040	139	6245	159	6450	163
5840	137	6045	148	6250	167	6455	166
5845	114	6050	140	6255	162	6460	143
5850	107	6055	147	6260	163	6465	166
5855	111	6060	152	6265	172	6470	144
5860	105	6065	133	6270	160	6475	168
5865	90	6070	139	6275	161	6480	178
5870	109	6075	141	6280	152	6485	166
5875	107	6080	134	6285	175	6490	169
5880	102	6085	147	6290	160	6495	171
5885	93	6090	153	6295	155	6500	168
5890	100	6095	148	6300	187	6505	171
5895	116	6100	135	6305	171	6510	164
5900	81	6105	133	6310	157	6515	186
5905	99	6110	150	6315	159		
5910	107	6115	165	6320	153		

Table S7 Stalagmite X3 grayscale data.

Age YBP	Grayscale	Age YBP	Grayscale	Age YBP	Grayscale	Age YBP	Grayscale	Age YBP	Grayscale
1024	142	1219	115	1414	112	1609	105	1804	130
1029	106	1224	93	1419	152	1614	121	1809	117
1034	116	1229	132	1424	150	1619	130	1814	118
1039	128	1234	117	1429	162	1624	147	1819	140
1044	138	1239	108	1434	119	1629	93	1824	145
1049	115	1244	146	1439	159	1634	137	1829	101
1054	121	1249	117	1444	179	1639	127	1834	128
1059	93	1254	153	1449	116	1644	133	1839	107
1064	149	1259	127	1454	135	1649	160	1844	103
1069	145	1264	119	1459	167	1654	160	1849	86
1074	143	1269	168	1464	144	1659	120	1854	136
1079	115	1274	162	1469	130	1664	133	1859	79
1084	73	1279	166	1474	126	1669	169	1864	98
1089	136	1284	168	1479	166	1674	97	1869	127
1094	130	1289	155	1484	105	1679	135	1874	101
1099	103	1294	123	1489	135	1684	114	1879	123
1104	110	1299	148	1494	126	1689	123	1884	127
1109	83	1304	172	1499	147	1694	143	1889	145
1114	136	1309	153	1504	149	1699	164	1894	137
1119	131	1314	152	1509	144	1704	134	1899	104
1124	121	1319	158	1514	121	1709	148	1904	101
1129	76	1324	149	1519	144	1714	164	1909	82
1134	116	1329	169	1524	116	1719	165	1914	121
1139	95	1334	171	1529	108	1724	144	1919	120
1144	127	1339	190	1534	154	1729	95	1924	97
1149	105	1344	145	1539	160	1734	128	1929	127
1154	120	1349	135	1544	133	1739	114	1934	136
1159	119	1354	125	1549	176	1744	131	1939	116
1164	134	1359	160	1554	137	1749	116	1944	102
1169	115	1364	169	1559	115	1754	84		
1174	112	1369	165	1564	168	1759	132		
1179	118	1374	153	1569	120	1764	103		
1184	91	1379	129	1574	92	1769	117		
1189	110	1384	139	1579	154	1774	132		
1194	119	1389	145	1584	119	1779	147		
1199	87	1394	147	1589	126	1784	125		
1204	137	1399	114	1594	108	1789	106		
1209	78	1404	139	1599	146	1794	147		

Table S8 Stalagmite X3 growth band thickness data.

Age YBP	Thickness (mm)	Age YBP	Thickness (mm)	Age YBP	Thickness (mm)	Age YBP	Thickness (mm)
1021	0.243	1060	0.334	1099	0.299	1138	0.283
1022	0.283	1061	0.324	1100	0.330	1139	0.252
1023	0.364	1062	0.304	1101	0.409	1140	0.299
1024	0.405	1063	0.162	1102	0.393	1141	0.252
1025	0.243	1064	0.182	1103	0.268	1142	0.330
1026	0.324	1065	0.283	1104	0.268	1143	0.283
1027	0.223	1066	0.375	1105	0.236	1144	0.268
1028	0.223	1067	0.375	1106	0.283	1145	0.268
1029	0.162	1068	0.364	1107	0.268	1146	0.378
1030	0.223	1069	0.314	1108	0.268	1147	0.315
1031	0.223	1070	0.385	1109	0.315	1148	0.330
1032	0.294	1071	0.456	1110	0.268	1149	0.283
1033	0.375	1072	0.415	1111	0.268	1150	0.393
1034	0.334	1073	0.516	1112	0.252	1151	0.315
1035	0.314	1074	0.415	1113	0.252	1152	0.330
1036	0.354	1075	0.314	1114	0.220	1153	0.409
1037	0.172	1076	0.283	1115	0.330	1154	0.409
1038	0.202	1077	0.354	1116	0.220	1155	0.362
1039	0.263	1078	0.324	1117	0.378	1156	0.268
1040	0.223	1079	0.294	1118	0.268	1157	0.205
1041	0.152	1080	0.334	1119	0.315	1158	0.378
1042	0.263	1081	0.364	1120	0.252	1159	0.393
1043	0.364	1082	0.283	1121	0.252	1160	0.346
1044	0.415	1083	0.405	1122	0.252	1161	0.252
1045	0.233	1084	0.364	1123	0.299	1162	0.472
1046	0.273	1085	0.425	1124	0.252	1163	0.283
1047	0.375	1086	0.294	1125	0.220	1164	0.456
1048	0.202	1087	0.304	1126	0.220	1165	0.393
1049	0.263	1088	0.334	1127	0.378	1166	0.441
1050	0.172	1089	0.273	1128	0.378	1167	0.393
1051	0.182	1090	0.252	1129	0.157	1168	0.315
1052	0.182	1091	0.220	1130	0.142	1169	0.173
1053	0.213	1092	0.315	1131	0.142	1170	0.173
1054	0.202	1093	0.236	1132	0.173	1171	0.157
1055	0.364	1094	0.252	1133	0.189	1172	0.220
1056	0.324	1095	0.252	1134	0.252	1173	0.205
1057	0.354	1096	0.299	1135	0.220	1174	0.252
1058	0.375	1097	0.299	1136	0.283	1175	0.268
1059	0.395	1098	0.205	1137	0.268	1176	0.268

1177	0.236	1216	0.426	1255	0.377	1294	0.340
1178	0.299	1217	0.365	1256	0.292	1295	0.170
1179	0.220	1218	0.341	1257	0.292	1296	0.276
1180	0.283	1219	0.377	1258	0.304	1297	0.340
1181	0.236	1220	0.426	1259	0.304	1298	0.319
1182	0.330	1221	0.317	1260	0.231	1299	0.340
1183	0.378	1222	0.475	1261	0.292	1300	0.340
1184	0.330	1223	0.499	1262	0.170	1301	0.276
1185	0.330	1224	0.365	1263	0.231	1302	0.276
1186	0.362	1225	0.329	1264	0.280	1303	0.297
1187	0.409	1226	0.329	1265	0.280	1304	0.255
1188	0.346	1227	0.341	1266	0.234	1305	0.234
1189	0.393	1228	0.292	1267	0.212	1306	0.276
1190	0.299	1229	0.329	1268	0.276	1307	0.255
1191	0.252	1230	0.329	1269	0.276	1308	0.255
1192	0.220	1231	0.292	1270	0.319	1309	0.234
1193	0.292	1232	0.317	1271	0.212	1310	0.276
1194	0.329	1233	0.280	1272	0.276	1311	0.212
1195	0.280	1234	0.317	1273	0.234	1312	0.276
1196	0.317	1235	0.317	1274	0.255	1313	0.276
1197	0.365	1236	0.292	1275	0.212	1314	0.297
1198	0.317	1237	0.268	1276	0.127	1315	0.276
1199	0.438	1238	0.268	1277	0.255	1316	0.297
1200	0.341	1239	0.268	1278	0.234	1317	0.255
1201	0.329	1240	0.219	1279	0.297	1318	0.234
1202	0.231	1241	0.280	1280	0.319	1319	0.234
1203	0.317	1242	0.341	1281	0.276	1320	0.234
1204	0.377	1243	0.304	1282	0.234	1321	0.212
1205	0.329	1244	0.304	1283	0.255	1322	0.170
1206	0.280	1245	0.256	1284	0.255	1323	0.276
1207	0.365	1246	0.268	1285	0.361	1324	0.234
1208	0.329	1247	0.341	1286	0.276	1325	0.255
1209	0.414	1248	0.231	1287	0.297	1326	0.234
1210	0.329	1249	0.244	1288	0.212	1327	0.191
1211	0.280	1250	0.292	1289	0.255	1328	0.191
1212	0.390	1251	0.244	1290	0.297	1329	0.212
1213	0.377	1252	0.438	1291	0.255	1330	0.212
1214	0.377	1253	0.390	1292	0.212	1331	0.212
1215	0.353	1254	0.329	1293	0.212	1332	0.361
1333	0.212	1372	0.234	1411	0.319	1450	0.292
1334	0.234	1373	0.276	1412	0.361	1451	0.324
1335	0.234	1374	0.255	1413	0.361	1452	0.373
1336	0.234	1375	0.255	1414	0.405	1453	0.357

1337	0.276	1376	0.255	1415	0.243	1454	0.324
1338	0.276	1377	0.255	1416	0.276	1455	0.373
1339	0.319	1378	0.340	1417	0.292	1456	0.292
1340	0.276	1379	0.297	1418	0.227	1457	0.373
1341	0.212	1380	0.382	1419	0.276	1458	0.357
1342	0.276	1381	0.319	1420	0.276	1459	0.292
1343	0.234	1382	0.403	1421	0.292	1460	0.373
1344	0.297	1383	0.319	1422	0.373	1461	0.292
1345	0.297	1384	0.276	1423	0.308	1462	0.308
1346	0.234	1385	0.255	1424	0.243	1463	0.405
1347	0.276	1386	0.276	1425	0.276	1464	0.357
1348	0.276	1387	0.340	1426	0.243	1465	0.405
1349	0.191	1388	0.340	1427	0.243	1466	0.308
1350	0.212	1389	0.319	1428	0.405	1467	0.178
1351	0.212	1390	0.403	1429	0.389	1468	0.243
1352	0.276	1391	0.276	1430	0.259	1469	0.211
1353	0.276	1392	0.297	1431	0.211	1470	0.227
1354	0.212	1393	0.340	1432	0.259	1471	0.259
1355	0.149	1394	0.276	1433	0.292	1472	0.276
1356	0.149	1395	0.212	1434	0.259	1473	0.308
1357	0.212	1396	0.297	1435	0.211	1474	0.292
1358	0.170	1397	0.255	1436	0.178	1475	0.259
1359	0.149	1398	0.297	1437	0.454	1476	0.422
1360	0.234	1399	0.319	1438	0.308	1477	0.324
1361	0.191	1400	0.297	1439	0.389	1478	0.292
1362	0.276	1401	0.319	1440	0.276	1479	0.422
1363	0.255	1402	0.425	1441	0.259	1480	0.389
1364	0.212	1403	0.319	1442	0.227	1481	0.373
1365	0.191	1404	0.382	1443	0.292	1482	0.308
1366	0.234	1405	0.340	1444	0.292	1483	0.259
1367	0.255	1406	0.361	1445	0.292	1484	0.373
1368	0.255	1407	0.361	1446	0.243	1485	0.324
1369	0.276	1408	0.297	1447	0.324	1486	0.324
1370	0.212	1409	0.340	1448	0.373	1487	0.341
1371	0.255	1410	0.297	1449	0.324	1488	0.470
1489	0.373	1528	0.210	1567	0.245	1606	0.193
1490	0.422	1529	0.298	1568	0.298	1607	0.245
1491	0.308	1530	0.245	1569	0.228	1608	0.245
1492	0.341	1531	0.385	1570	0.193	1609	0.210
1493	0.535	1532	0.333	1571	0.228	1610	0.298
1494	0.308	1533	0.368	1572	0.245	1611	0.263
1495	0.211	1534	0.333	1573	0.245	1612	0.193
1496	0.276	1535	0.298	1574	0.315	1613	0.228

1497	0.259	1536	0.315	1575	0.298	1614	0.245
1498	0.178	1537	0.368	1576	0.193	1615	0.245
1499	0.389	1538	0.455	1577	0.193	1616	0.368
1500	0.357	1539	0.298	1578	0.123	1617	0.298
1501	0.227	1540	0.385	1579	0.158	1618	0.263
1502	0.243	1541	0.280	1580	0.175	1619	0.245
1503	0.259	1542	0.368	1581	0.140	1620	0.403
1504	0.341	1543	0.298	1582	0.263	1621	0.350
1505	0.470	1544	0.298	1583	0.228	1622	0.333
1506	0.519	1545	0.368	1584	0.298	1623	0.333
1507	0.227	1546	0.298	1585	0.315	1624	0.263
1508	0.389	1547	0.333	1586	0.315	1625	0.319
1509	0.373	1548	0.315	1587	0.350	1626	0.331
1510	0.405	1549	0.368	1588	0.210	1627	0.307
1511	0.195	1550	0.280	1589	0.228	1628	0.245
1512	0.259	1551	0.263	1590	0.333	1629	0.258
1513	0.227	1552	0.333	1591	0.420	1630	0.393
1514	0.175	1553	0.210	1592	0.333	1631	0.466
1515	0.210	1554	0.245	1593	0.350	1632	0.527
1516	0.491	1555	0.280	1594	0.385	1633	0.552
1517	0.263	1556	0.350	1595	0.403	1634	0.454
1518	0.385	1557	0.333	1596	0.385	1635	0.417
1519	0.403	1558	0.508	1597	0.455	1636	0.724
1520	0.403	1559	0.245	1598	0.438	1637	0.442
1521	0.420	1560	0.280	1599	0.315	1638	0.393
1522	0.385	1561	0.210	1600	0.368	1639	0.466
1523	0.368	1562	0.298	1601	0.315	1640	0.331
1524	0.368	1563	0.280	1602	0.315	1641	0.466
1525	0.455	1564	0.263	1603	0.333	1642	0.503
1526	0.280	1565	0.280	1604	0.333	1643	0.380
1527	0.228	1566	0.228	1605	0.228	1644	0.478
1645	0.429	1684	0.218	1723	0.259	1762	0.179
1646	0.429	1685	0.300	1724	0.164	1763	0.194
1647	0.417	1686	0.300	1725	0.191	1764	0.298
1648	0.343	1687	0.300	1726	0.177	1765	0.298
1649	0.429	1688	0.273	1727	0.177	1766	0.298
1650	0.258	1689	0.273	1728	0.218	1767	0.358
1651	0.417	1690	0.286	1729	0.218	1768	0.328
1652	0.282	1691	0.259	1730	0.177	1769	0.373
1653	0.307	1692	0.218	1731	0.245	1770	0.373
1654	0.393	1693	0.273	1732	0.177	1771	0.224
1655	0.233	1694	0.232	1733	0.191	1772	0.238
1656	0.319	1695	0.300	1734	0.150	1773	0.268

1657	0.331	1696	0.300	1735	0.191	1774	0.268
1658	0.294	1697	0.341	1736	0.205	1775	0.298
1659	0.319	1698	0.355	1737	0.191	1776	0.224
1660	0.356	1699	0.355	1738	0.109	1777	0.253
1661	0.307	1700	0.300	1739	0.286	1778	0.283
1662	0.429	1701	0.327	1740	0.286	1779	0.268
1663	0.314	1702	0.286	1741	0.286	1780	0.253
1664	0.286	1703	0.300	1742	0.300	1781	0.328
1665	0.300	1704	0.259	1743	0.259	1782	0.283
1666	0.245	1705	0.314	1744	0.218	1783	0.268
1667	0.355	1706	0.205	1745	0.245	1784	0.268
1668	0.409	1707	0.273	1746	0.164	1785	0.268
1669	0.286	1708	0.232	1747	0.218	1786	0.238
1670	0.218	1709	0.286	1748	0.238	1787	0.328
1671	0.341	1710	0.368	1749	0.224	1788	0.268
1672	0.368	1711	0.286	1750	0.238	1789	0.238
1673	0.395	1712	0.314	1751	0.238	1790	0.268
1674	0.300	1713	0.232	1752	0.283	1791	0.253
1675	0.245	1714	0.191	1753	0.328	1792	0.209
1676	0.218	1715	0.259	1754	0.224	1793	0.179
1677	0.245	1716	0.259	1755	0.298	1794	0.298
1678	0.327	1717	0.300	1756	0.343	1795	0.209
1679	0.300	1718	0.177	1757	0.388	1796	0.224
1680	0.382	1719	0.245	1758	0.432	1797	0.268
1681	0.300	1720	0.191	1759	0.238	1798	0.253
1682	0.341	1721	0.232	1760	0.358	1799	0.268
1683	0.259	1722	0.150	1761	0.298	1800	0.298
1801	0.328	1840	0.268	1879	0.406	1918	0.237
1802	0.283	1841	0.209	1880	0.305	1919	0.220
1803	0.298	1842	0.298	1881	0.305	1920	0.152
1804	0.268	1843	0.417	1882	0.152	1921	0.457
1805	0.298	1844	0.238	1883	0.220	1922	0.254
1806	0.328	1845	0.328	1884	0.254	1923	0.338
1807	0.298	1846	0.373	1885	0.271	1924	0.355
1808	0.313	1847	0.388	1886	0.254	1925	0.338
1809	0.328	1848	0.358	1887	0.338	1926	0.271
1810	0.462	1849	0.373	1888	0.237	1927	0.389
1811	0.343	1850	0.492	1889	0.271	1928	0.541
1812	0.313	1851	0.402	1890	0.203	1929	0.322
1813	0.388	1852	0.305	1891	0.203	1930	0.440
1814	0.447	1853	0.305	1892	0.254	1931	0.355
1815	0.417	1854	0.338	1893	0.254	1932	0.305
1816	0.268	1855	0.305	1894	0.237	1933	0.254

1817	0.283	1856	0.305	1895	0.389	1934	0.288
1818	0.388	1857	0.271	1896	0.288	1935	0.389
1819	0.388	1858	0.288	1897	0.288	1936	0.322
1820	0.522	1859	0.237	1898	0.220	1937	0.355
1821	0.492	1860	0.322	1899	0.355	1938	0.288
1822	0.388	1861	0.288	1900	0.457	1939	0.288
1823	0.432	1862	0.305	1901	0.305	1940	0.271
1824	0.402	1863	0.322	1902	0.389	1941	0.288
1825	0.447	1864	0.271	1903	0.305	1942	0.338
1826	0.462	1865	0.305	1904	0.305	1943	0.372
1827	0.388	1866	0.305	1905	0.389	1944	0.305
1828	0.283	1867	0.271	1906	0.423	1945	0.271
1829	0.373	1868	0.254	1907	0.305	1946	0.322
1830	0.328	1869	0.254	1908	0.305	1947	0.457
1831	0.283	1870	0.288	1909	0.254	1948	0.288
1832	0.402	1871	0.254	1910	0.237		
1833	0.328	1872	0.254	1911	0.220		
1834	0.238	1873	0.288	1912	0.220		
1835	0.298	1874	0.271	1913	0.271		
1836	0.343	1875	0.254	1914	0.220		
1837	0.253	1876	0.288	1915	0.254		
1838	0.194	1877	0.355	1916	0.254		
1839	0.238	1878	0.372	1917	0.203		

REFERENCES

Adams, D., and Comrie, A., 1997: The North American Monsoon. *Bulletin of the American Meteorological Society* **78**, 2197-2213.

An, C., Tang, L., Barton, L., and Chen, F., 2005: Climate change and cultural response around 4000 cal yr B.P. in the western part of Chinese Loess Plateau. *Quaternary Research* **63**, 347-352.

An, S., Kug, J., Ham, Y., and Kang, I., 2008: Successive modulation of ENSO to the future greenhouse warming. *Journal of Climate* **21**, 3-21.

Anderson, R., 1993: A 35,000 year vegetation and climate history from Potato Lake, Mogollon Rim, Arizona. *Quaternary Research* **40**, 351-359.

Anderson, R., Jass, R., Toney, J., Allen, C., Cisneros-Dozal, L., Hess, M., Heikoop, J., and Fessenden, J., 2008: Development of the mixed conifer forest in northern New Mexico and its relationship to Holocene environmental change. *Quaternary Research* **69**, 263-275.

Antevs, E., 1955: Geologic-climatic dating in the West. *American Antiquity* **20**, 317-335.

Asmerom, Y., Polyak, V., Schwieters, J., Bouman, C., 2006: Routine high-precision U-Th isotope analyses for paleoclimate chronology. *Geochimica et Cosmochimica Acta* **70**, A24.

Asmerom, Y., Polyak, V., Burns, S., and Rassmussen, J., 2007: Solar forcing of Holocene climate: New insights from a speleothem record, southwestern United States. *Geology* **35**, 1-4.

Asmerom, Y., Polyak, V., and Burns, S., 2010: Variable winter moisture in the southwestern United States linked to rapid glacial climate shifts. *Nature Geoscience* **3**, 114-117.

Asmerom, Y., Polyak, V., Rasmussen, J., Burns, S., and Lachniet, M., 2013: Multidecadal to multicentury scale collapses of Northern Hemisphere monsoons over the past millennium. *PNAS* **110**, 9651-9656.

Ayalon, A., Bar-Matthews, M., and Kaufman, A., 1999: Petrography, strontium, barium and uranium concentrations, and strontium and uranium isotope ratios in speleothems as palaeoclimatic proxies: Soreq Cave, Israel. *The Holocene* **9**, 715-722.

Banner, J., 1995: Application of the trace element and isotope geochemistry of strontium to studies of carbonate diagenesis. *Sedimentology* **42**, 805-824.

Barron, J., Heusser, L., Herbert, T., and Lyle, M., 2003: High-resolution climatic evolution of coastal northern California during the past 16,000 years. *Paleoceanography* **18**, 1, 1020, doi:10.1029/2002PA000768.

Barron, J., and Anderson, L., 2011: Enhanced Late Holocene ENSO/PDO expression along the margins of the eastern North Pacific. *Quaternary International* **30**, 1-10.

Berger, A. and Loutre, M., 1991: Insolation values for the climate of the last 10 million years. *Quaternary Sciences Review* **10**, 4, 297-317.

Betancourt, J., Pierson, E., Rylander, K., Fairchild-Parks, J., and Dean, J., 1993: *Influence of history and climate on New Mexico pinon-juniper woodlands*. In: Aldon, E.F. and D.W. Shaw, eds., Managing pinyon-juniper ecosystems for sustainability and social needs. USDA, Forest Service, GTR-RM-236, p. 42-62.

Betancourt, J., Rylander, K., Penalba, C., and McVickar, J., 2001: Late Quaternary vegetation history of Rough Canyon, south-central New Mexico, USA. *Palaeogeography, Palaeoclimatology, Palaeoecology* **165**, 71-95.

Booth, R., Jackson, S., Forman, S., Kutzbach, J., Bettis, E., Kreig, J., and Wright, D., 2005: A severe centennial-scale drought in mid-continental North America 4200 years ago and apparent global linkages. *The Holocene* **15**, 321-328.

Chen, F., Xu, Q., Chen, J., Birks, J., Liu, J., Zhang, S., Jin, L., An, C., Telford, R., Cao, X., Wang, Z., Zhang, X., Selvaraj, K., Lu, J., Li, Y., Zheng, Z., Wang, H., Zhou, A., Dong, G., Zhang, J., Huang, X., Bloemendal, J., and Rao, Z, 2015: East Asian summer monsoon precipitation variability since the last deglaciation: Scientific Reports.

Cheng, H., Lawrence Edwards, R., Shen C., Polyak, V., Asmerom, Y., Woodhead, J., Hellstrom, J., Wang, Y., Kong, X., Spotl, C., Wang, X., Calvin Alexander, E., 2013: Improvements in 230Th dating, 230Th and 234U half-life values, and U-Th isotopic measurements by multi-collector inductively coupled plasma mass spectrometry. *Earth and Planetary Science Letters* **371-372**, 82-91.

Clement, A., Seager, R., and Cane, M., 2000: Suppression of El Nino during the mid-Holocene by changes in the Earth's orbit. *Paleoceanography* **15**, 731-737.

Cole, J., and Cook, E., 1998: The changing relationship between ENSO variability and moisture balance in the continental United States. *Geophysical Research Letters* **25,** 4529-4532.

Collins, M., An, S., Cai, W., Ganachaud, A., Guilyardi, E., Jin, F., Jochum, M., Lengaigne, M., Power, S., Timmerman, A., Vecchi, G., and Wittenberg, A., 2010: The impact of global warming on the tropical Pacific Ocean and El Nino. *Nature Geoscience* **3**, 391-397.

Conroy, J., Overpeck, J., Cole, J., Shanahan, T., and Steinitz-Kannan, M., 2008: Holocene changes in eastern tropical Pacific climate inferred from a Galapagos lake sediment record. *Quaternary Science Reviews* **27**, 1166-1180.

Cook, E., Seager, R., Cane, M., and Stahle, D., 2007: North American drought: Reconstructions, causes, and consequences. *Earth-Science Reviews* **81**, 93-134.

Dai, A., 2013: Increasing drought under global warming in observations and models. *Nature Climate Change* **3**, 52-58.

deMenocal, P., 2001: Cultural responses to climate change during the Late Holocene. *Science* **292**, 667-673.

Fairchild, I., Borsato, A., Tooth, A., Frisia, S., Hawkesworth, C., Huang, Y., McDermott, F., Spiro B., 2000: Controls on trace element (Sr-Mg) compositions of carbonate cave waters: implications for speleothem climatic records. *Chemical Geology* **166**, 255-269.

Fairchild, I., and Treble, P., 2009: Trace elements in speleothems as recorders of environmental change. *Quaternary Science Reviews* **28**, 449-468.

Feng, X., and Epstein, S., 1994: Climatic implications of an 8000-year Hydrogen isotope time series from bristlecone pine trees. *Science* **265**, 1079-1081.

Gliganic, L., Cohen, T., May, J., Jansen, J., Nanson G., Dosseto, A., Larsen, J., and Aubert, M., 2014: Late-Holocene climatic variability indicated by three natural archives in arid southern Australia. *The Holocene* **24,** 104-117.

Graham, N., 2004: Late-Holocene teleconnections between tropical Pacific climatic variability and precipitation in the western USA: evidence from proxy records. *The Holocene* **14**, 436-447.

Gray, S., Betancourt, J., Fastie, C., and Jackson, S., 2003: Patterns and sources of multidecadal oscillations in drought-sensitive tree-ring records from the central and southern Rocky Mountains. *Geophysical Research Letters* **30.**

Grissino-Mayer, H., Swetnam, T., and Adams, R., 1997: The rare, old-aged conifers of El Malpais- Their role in understanding climatic change in the American Southwest. *New Mexico Bureau of Mines & Mineral Resources, Bulletin* **156**, 155-161.

Haug, G., Gunther, D., Peterson, L., Sigman, D., Hughen, K., and Aeschlimann, B., 2003: Climate and the collapse of the Maya civilization. *Science* **299**, 1731-1735.

He, X., and Guan, H., 2013: Multiresolution analysis of precipitation teleconnections with large-scale climate signals: A case study in South Australia. *Water Resources Research* **49**, 6995-7008.

Hill, C., 1987: Geology of Carlsbad Cavern and other caves in the Guadalupe Mountains, New Mexico and Texas. *New Mexico Bureau of Mines & Mineral Resources Bulletin* **117,** 150 p.

Hill, C., 2000: Overview of the Geologic History of Cave Development in the Guadalupe Mountains, New Mexico. *Journal of Cave and Karst Studies* **62**, 60-71.

Hodell, D., Curtis, J., and Brenner, M., 1995: Possible role of climate in the collapse of Classic Maya civilization. *Nature* **375**, 391-394.

Jagnow, D., Hill, C., Davis, D., DuChene, H., Cunningham, K., Northup, D., Queen, J., 2000: History of the sulfuric acid theory of speleogenesis in the Guadalupe Mountains, New Mexico. *Journal of Cave and Karst Studies* **62,** 54-59.

Jiang, W., Guo, Z., Sun, X., Wu H., Chu, G., Yuan, B., Hatte, C., and Guiot, J., 2006: Reconstruction of climate and vegetation changes of Lake Bayanchagan (inner Mongolia): Holocene variability of the East Asian monsoon. *Quaternary Research* **65**, 411-420.

Knox, J., 1993: Large increases in flood magnitude in response to modest climate. Nature **361**, 430-432.

Kirby, M., Knell, E., Anderson, W., Lachniet, M., Palermo, J., Eeg, H., Lucero, R., Murrieta, R., Arevalo, A., Silveira, E., and Hiner, C., 2015: Evidence for insolation and Pacific forcing of late glacial through Holocene climate in the Central Mojave Desert (Silver Lake, CA). *Quaternary Research* **84**, 174-186.

Knudsen, M., Seidenkrantz, M., Jacobsen, B., and Kuijpers, A., 2011: Tracking the Atlantic Multidecadal Oscillation through the last 8,000 years. *Nature Communications* **2**, no. 178.

Lachniet, M., 2009: Climatic and environmental controls on speleothem oxygen-isotope values. *Quaternary Science Reviews* **28**, 412-432.

Lachniet, M., Denniston, R., Asmerom, Y., and Polyak, V., 2014: Orbital control of western North America atmospheric circulation and climate over two glacial cycles. *Nature Communications* **5**, 3805.

LaMarche, V., 1973: Holocene climatic variations inferred from treeline fluctuations in the White Mountains, California. *Quaternary Research* **3**, 632-660.

Liu, Z., Lutzbach, J., and Wu, L., 2000: Modeling climate shift of El Nino variability in the Holocene. *Geophysical Research Letters* **27**, 2265-2268.

Liu, Z., Otto-Bliesner, B., Kutzbach, J., Li, L., and Shields, C., 2003: Coupled climate simulation of the evolution of global monsoons in the Holocene. *Journal of Climate* **16**, 2472-2490.

Marcott, S., Shakun, J., Clark, P., and Mix, A, 2013: A reconstruction of regional and global temperature for the past 11,300 years. *Science* **339**, 1198-1201.

Mayewski, P., Rohling, E., Stager, J., Karlen, W., Maasch, K., Meeker, L., Meyerson, E., Gasse, F., van Kreveld, S., Holmgren, K., Lee-Thorp, J., Rosqvist, G., Rack, F., Staubwasser, M., Schneider, R., Steig, E., 2004: Holocene climate variability. *Quaternary Research* **62**, 243-255.

McDermott, F., 2004: Palaeo-climate reonstruction from stable isotope variations in speleothems: a review. *Quaternary Science Reviews* **23**, 901-918.

McCabe, G., Palecki, M., and Betancourt, J., 2004: Pacific and Atlantic Ocean influences on multidecadal drought frequency in the United States. *PNAS* **101,** 4136-4141.

McLean, J., 1971: The microclimate in Carlsbad Caverns, New Mexico. *U.S. Geological Survey, Open File Report,* 76-171, 55 pp.

Menking, K., and Anderson, R., 2003: Contributions of La Nina and El Nino to middle Holocene and late Holocene moisture in the American Southwest. *Geology* **31**, 937-940.

Merrill, W., Hard, R., Mabry, J., Fritz, G., Adams, K., Roney, J., and MacWilliams, A., 2009: The diffusion of maize to the southwestern United States and its impact. *PNAS* **106**, 21019-21026.

Metcalfe, S., Barron, J., and Davies, S., 2015: The Holocene history of the North American Monsoon: ‘known knowns’ and ‘known unknowns’ in understanding its spatial and temporal complexity. *Quaternary Science Reviews* **120**, 1-27.

Minobe, S., 1997: A 50-70 year climatic oscillation over the North Pacific and North America. *Geophysical Research Letters* **24**, 683-686.

Ogurtsov, M., Nagovitsyn, Y., Kocharov, G., and Jungner, H., 2002: Long-period cycles of the sun’s activity recorded in direct solar data and proxies. *Solar Physics* **211**, 371-394.

Polyak, V., and Asmerom, Y., 2001: Late Holocene climate and cultural changes in the southwestern United States. *Science* **294**, 148-150.

Polyak, V.J., Cokendolpher, J., Norton, R., and Asmerom, Y., 2001: Wetter and cooler late Holocene climate in the southwestern United States from mites preserved in stalagmites. *Geology* **29**, 643-646.

Polyak, V., Asmerom, Y., Burns, S., and Lachniet, M., 2012: Climatic backdrop to the terminal Pleistocene extinction of North American mammals. *Geology* **40**, 1023-1026.

Poore, R., Pavich, M., and Grissino-Mayer, H., 2005: Record of the North American monsoon from Gulf of Mexico sediment cores. *Geology* **33**, 209-212.

Railsback, L., Brook, G., Chen, J., Kalin, C., and Fleisher, C., 1994: Environmental controls on the petrology of a Late Holocene speleothem from Botswana with annual layers of aragonite and calcite. *Journal of Sedimentary Research Section a- Sedimentary Petrology and Processes* **64**, 147-155.

Rasmussen, J., 2006: Late Holocene climate variability in the Southwestern United States from high-resolution speleothem data [*PhD dissertation*]: University of New Mexico, 199 p.

Rasmussen, J., Polyak, V., and Asmerom, Y., 2006: Evidence for Pacific-modulated precipitation variability during the late Holocene from southwestern USA. *Geophysical Research Letters* **33**.

Rasmussen, S., Bigler, M., Blockley, S., Blunier, T., Buchardt, S., Clausen, H., Cvijanovic, I., Dahl-Jenson, D., Johnsen, S., Fischer, H., Gkinis, V., Guillevic, M., Hoek, W., Lowe, J., Pedro, J., Popp, T., Seierstad, I., Steffensen, J., Svensson, A., Vallelonga, P., Vinther, B., Walker, M., Wheatley, J., and Winstrup, M., 2014: A stratigraphic framework for abrupt climatic changes during the Last Glacial period based on three synchronized Greenland ice-core records: refining and extending the INTIMATE event stratigraphy. *Quaternary Science Reviews*, **106**, 14-28.

Renssen, H., Seppa, H., Crosta, X., Goosse, H., and Roche, D., 2012: Global characterization of the Holocene Thermal Maximum. *Quaternary Science Reviews* **48**, 7-19.

Sadekov, A., Ganeshram, R., Pichevin, L., Berdin, R., McClymont, E., Elderfield, H., and Tudhope, A., 2013: Palaeoclimate reconstructions reveal a strong link between El Nino-Southern Oscillation and Tropical Pacific mean state. *Nature Communications* **4**:2692.

Scaife, A., Ineson, S., Knight, J., Gray, L., Kodera, K., and Smith, D., 2013: A mechanism for lagged North Atlantic climate response to solar variability. *Geophysical Research Letters* **40**, 434-439.

Schulz and Mudelsee, 2002: REDFIT: estimating red-noise spectra directly from unevenly spaced paleoclimatic time series. *Computers & Geosciences* **28**, 421-426.

Scuderi, L., 1987: Late-Holocene upper timberline variation in the southern Sierra Nevada. *Nature* **325**, 242-244.

Sharp, Z., 2007: *Principles of Stable Isotope Geochemistry.* Pearson Education, Inc., 344 p.

Sheppard, P., Comrie, A., Packin, G., Andersbach, K., and Hughes, M., 2002: The climate of the US Southwest. *Climate Research* **21**, 219-238.

Sonett, C., and Finney, S., 1990: The spectrum of radiocarbon: The Earth's Climate and Variability of the Sun Over Recent Millennia. *Geophysical, Astronomical and Archaeological Aspects* **330**, 413-426.

Timmermann, A., Oberhuber, J., Bacher, A., Esch, M., Latif, M., and Roeckner, E., 1999: Increased El Nino frequency in a climate model forced by future greenhouse warming. *Nature* **398**, 694-697.

Torrence, C., and Compo, G., 1998: A practical guide to wavelet analysis. *Bulletin of the American Meteorological Society* **79**, 61-78.

Tremaine, D., and Froelich, P., 2013: Speleothem trace element signatures :A hydrologic geochemical study of modern cave dripwaters and farmed calcite. *Geochimica et Cosmochimica Acta* **121**, 522-545.

Vecchi, G., Soden, B., Wittenberg, A., and Harrison, M., 2006: Weakening of tropical Pacific atmospheric circulation due to anthropogenic forcing. *Nature* **441**, 73-76.

Walker, M., Berkelhammer, M., Bjork, S., Cwyner, L., Fisher, D., Long, A., Lowe, J., Newnham, R., Rasmussen, S., Weiss, H., 2012: Formal subdivision of the Holocene Series/Epoch: a discussion paper by a working group of INTIMATE (Integration of ice-core, marine, and terrestrial records) and the subcommission on Quaternary stratigraphy (International Commission on Stratigraphy). *Journal of Quaternary Science* **27**, 649-659.

Wang, Y., Cheng, H., Edwards, L., He, Y., Kong, X., An, Z., Wu, J., Kelly, M., Dykosko, C., and Li, X, 2005: The Holocene Asian monsoon: links to solar changes and North Atlantic Climate. *Science* **308**, 854-856.

Wang, S., Huang, J., He, Y., and Guan, Y., 2014: Combined effects of the Pacific Decadal Oscillation and the El Nino-Southern Oscillation on global land dry-wet changes. *Scientific Reports* **4**:6651.

Wanner, H., Beer, J., Butikofer, J., Crowley, T., Cubasch, U., Fluckiger, J., Goosse, H., Grosjean, M., Joos, F., Kaplan, J., Kuttel, M., Muller, S., Prentice, I., Solomina, O., Stocker, T., Tarasov, P., Wagner, M., and Widmann, M., 2008: Mid to Late

Holocene climate change: an overview. *Quaternary Science Reviews* **27**, 1791-1828.

Waters, M., and Haynes, C., 2001: Late Quaternary arroyo formation and climate change in the American Southwest. *Geology* **29**, 399-402.

Woodhouse, C., Meko, D., MacDonald, G., Stahle, D., and Cook, E., 2009: A 1,200-year perspective of 21st century drought in southwestern North America. *PNAS* **107**, 21283-21288.

Yang, X., Scuderi, L., Wang, X., Scuderi, L., Zhang, D., Li, H., Forman, S., Xu, Q., Wang, R., Huang, W., Yang, S., 2015: Groundwater sapping as the cause of irreversible desertification of Hunshandake Sandy Lands, Inner Mongolia, northern China. *PNAS* **112**, 702-706.

Zhou, J., Lundstrom, C., Fouke, B., Panno, S., Hackley, K., and Curry, B., 2005: Geochemistry of speleothem records from southern Illinois: Development of (234U)/(238U) as a proxy for paleoprecipitation. *Chemical Geology* **221**, 1-20.